



Recent Progress of Cardiac MRI for Nuclear Medicine Professionals

Yeon Hyeon Choe¹ · Sung Mok Kim¹

Received: 16 October 2023 / Revised: 31 January 2024 / Accepted: 4 February 2024
© The Author(s), under exclusive licence to Korean Society of Nuclear Medicine 2024

Abstract

Recent technical innovation enables faster and more reliable cardiac magnetic resonance (CMR) imaging than before. Artificial intelligence is used in improving image resolution, fast scanning, and automated analysis of CMR. Fast CMR techniques such as compressed sensing technique enable fast cine, perfusion, and late gadolinium-enhanced imaging and improve patient throughput and widening CMR indications. CMR feature-tracking technique gives insight on diastolic function parameters of ventricles and atria with prognostic implications. Myocardial parametric mapping became to be included in the routine CMR protocol. CMR fingerprinting enables simultaneous quantification of myocardial T1 and T2. These parameters may give information on myocardial alteration in the preclinical stages in various myocardial diseases. Four-dimensional flow imaging shows hemodynamic characteristics in or through the cardiovascular structures visually and gives quantitative values of vortex, kinetic energy, and wall-shear stress. In conclusion, CMR is an essential modality in the diagnosis of various cardiovascular diseases, especially myocardial diseases. Recent progress in CMR techniques promotes more widespread use of CMR in clinical practice. This review summarizes recent updates in CMR technologies and clinical research.

Keywords Cardiac magnetic resonance (CMR) imaging · Techniques · Deep learning · Myocardial parametric mapping · Feature tracking · 4D flow

Abbreviations

AI	Artificial intelligence
CMR	Cardiac magnetic resonance imaging
CNN	Convolutional neural network
CAD	Coronary artery disease
DL	Deep learning
ECV	Extracellular volume fraction
HCM	Hypertrophic cardiomyopathy
LV	Left ventricular
MACE	Major adverse cardiac events
MF	Myocardial fibrosis
LGE	Late gadolinium enhancement
PET	Positron emission tomography
STEMI	ST-elevation myocardial infarction

Introduction

Cardiac magnetic resonance (CMR) imaging is the current gold standard for the evaluation of ventricular function, myocardial viability, and tissue characterization [1–4]. Myocardial parametric mapping is now being included as a routine CMR technique and helps further characterize myocardium beyond the capability of late gadolinium enhancement (LGE). Strain imaging with or without compressed-sensing cine MR imaging using feature tracking and deep-learning-based automated analysis allows rapid and easy assessment of ventricular and atrial strains. Artificial intelligence (AI) and deep learning (DL) are applied to every step of image acquisition, postprocessing, and image analysis in various sequences of CMR. Four-dimensional (4D) flow, positron emission tomography (PET)-MR, diffusion imaging, and radiomics are already established techniques and have increasingly attracted the attention of radiologists and clinicians [4–16]. Recent CMR technical innovations and related clinical applications are summarized in Table 1.

✉ Yeon Hyeon Choe
yhchoe@skku.edu

¹ Department of Radiology and Center for Imaging Science, Heart Vascular Stroke Institute, Samsung Medical Center, Sungkyunkwan University School of Medicine, 81 Irwonro, Gangnam-Gu, Seoul 06351, South Korea

Table 1 Technical innovations and related clinical applications in CMR

Technical innovations	Related clinical applications
Artificial intelligence Image data acquisition Image analysis	All indications of CMR
MR fingerprinting Parametric mapping	Myocardial diseases, all
4D flow	Aortic disease, valvular heart disease, Fontan operation, hypertrophic cardiomyopathy
Diffusion imaging	Myocardial infarction, hypertrophic cardiomyopathy
Radiomics Late Gd enhancement Parametric mapping	Myocardial infarction, hypertrophic cardiomyopathy, cardiac tumors and thrombus
PET/MRI	Myocardial infarction, sarcoidosis
Strain imaging	Myocardial diseases, all
Compressed sensing Cine Strain imaging Coronary MR angiography 4D flow	All indications of CMR
Late gadolinium enhancement Dark-blood 3D high-spatial-resolution imaging	Atrial fibrillation, myocardial infarction
Ferumoxitol (Feraheme) Coronary MR angiography	Coronary artery disease
7 T CMR ³¹ P-MR spectroscopy	Myocardial disease

Recent Developments in CMR Techniques

Artificial Intelligence

DL enables automatic detection of cardiac phases, cardiac segmentation, left ventricular quantification, cardiac motion tracking, cardiac strain analysis, myocardial perfusion, detection and assessment of myocardial regions with infarction, and discrimination of hypertrophic cardiomyopathy from hypertensive heart disease [17–23]. Convolutional neural network (CNN) application on k-space acceleration and faster perfusion image reconstruction are an attractive approach [24].

Unal et al. proposed an automatic approach enabled by deep learning for detecting dark-rim artifacts (DRA) in first-pass perfusion CMR datasets [25]. The new algorithm can automatically detect DRA in individual time frames by analyzing multiple reconstructions of the same time frame (k-space data) with varying temporal windows. It can also suppress the extent and severity of DRAs. The method demonstrated good performance in detecting subendocardial DRAs in patients with suspected ischemic heart disease. The successful preliminary applications of DL in stress perfusion CMR are expected to improve diagnostic accuracy [18].

Compressed sensing (CS) and AI-cine can be used to obtain cine imaging covering the whole heart in a single

breath-hold. They showed the potential to complement the conventional cine MR imaging in the evaluation of biventricular function in patients with difficulties in holding breaths [26].

DL-based correction of motion artifacts is feasible. Kustner et al. performed retrospective motion correction using generative adversarial network to correct artifacts caused by cardiac motion or respiration with high evaluation metrics (normalized mean squared error, 0.08) [27].

Fahmy et al. proposed a CNN-based DL model for combining LGE and cine images for improving the quantification of myocardial fibrosis (MF) in patients with hypertrophic cardiomyopathy [28]. Supervised learning methods have been successful in the automated segmentation of MF [29]. 3D LGE incorporating ML algorithms enables fast characterization of MF.

In patients with heart failure with reduced ejection fraction (HFrEF), a DL-based multi-data denoising autoencoder model based on clinical datasets, popular CMR characteristics, and cardiac motion enables accurate survival prediction and risk stratification. It exhibited better prognostic value compared with conventional Cox hazard prediction models [30].

Myocardial Parametric Mapping

Myocardial T1, T2, T2* parametric mapping has emerged as an invaluable tools in the evaluation of various cardiac

diseases such as myocarditis, myocardial infarction, amyloidosis, heart failure, iron-overload disease, cardiac tumors, and Fabry disease [31–38] (Fig. 1). Parametric MR relaxation mapping methods are quantitative techniques that provide numerical T1 or T2 values in milliseconds [39]. Quantitative parametric mapping can detect diffuse disease without the need for contrast media. This technique allows the comparison of maps within individuals longitudinally over time [40]. MR sequences for cardiac T1-mapping are inversion-recovery, saturation-recovery or combinations of inversion-recovery, and saturation-recovery sequences with inversion-recovery-based T1-mapping techniques being the most common.

Native T1 values result from signals from both the intracellular and extracellular compartments of organs and can be affected by MR hardware and physiologic factors [39]. T1-mapping has shown the capability to detect abnormalities not detectable by LGE in patients with cardiomyopathy. In patients with suspected cardiomyopathy, T1 and T2 parametric mapping improved diagnostic confidence in 39% and higher sensitivity in myocarditis (89% vs 69%), Fabry disease (93% vs 50%), and amyloidosis (100% vs 63%) with mapping [41]. T1 mapping may be sensitive in the diagnosis of hemochromatosis even in cases with normal T2* values. T1 mapping can also differentiate Anderson-Fabry disease from other phenotypes of left ventricular hypertrophy by demonstrating low signal intensity from sphingolipid accumulation in the hypertrophied myocardium.

Myocardial ECV is calculated by multiplying the ratio of the pre- and post-contrast relaxivity ($R1 = 1/T1$) changes in the myocardium and blood ($\Delta R1_{\text{myocardium}}/\Delta R1_{\text{blood}}$) by the extracellular volume of blood (1-hematocrit). An equilibrium-CMR technique is based on a continuous infusion of

gadolinium contrast media longer than 30 min. Instead, in the dynamic-equilibrium method, ECV can be measured by T1-mapping before and 10 or 15 min after the administration of gadolinium contrast media. ECV may be increased due to diffuse interstitial fibrosis, amyloidosis, and edema and expansion of the intravascular compartment by coronary vasodilation [39].

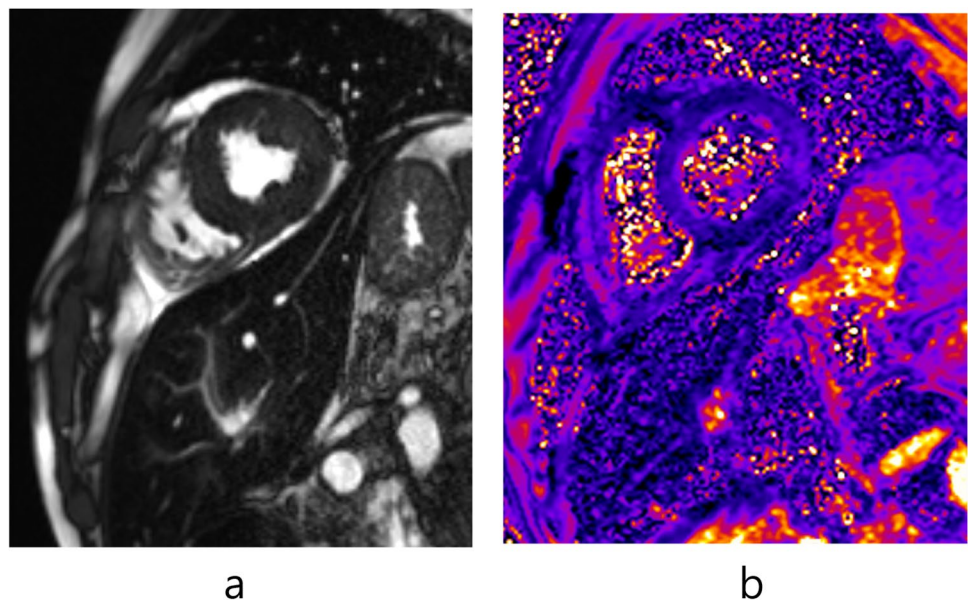
T2 mapping sequences include single-shot balanced steady-state free precession (bSSFP) acquisitions with different T2 preparation times, gradient and spin echo (GraSE), or fast spin echo (FSE)-based pulse sequences. The Consensus Statement of The Society for Cardiovascular Magnetic Resonance (SCMR) Mapping recommends T2-prepared bSSFP or gradient echo pulse sequences with a minimum of three differently T2-weighted images [42]. Myocardial T2 values depend on hardware, software, and physiologic factors (sex, age, and heart rates). T2 mapping is especially useful for the diagnosis of acute myocarditis showing inflammation/edema. T1 and T2 quantifications are now recommended for detecting myocardial inflammation [34, 43].

Automated mapping segmentation and calculation and fast 3-dimensional approaches with breath-holds or free breathing provide efficient work-flow for CMR [44–47].

T1 ρ (spin–lattice relaxation time in the rotating frame) mapping has emerged as a promising biomarker for quantifying myocardial abnormalities [48]. T1 ρ is sensitive to slow molecular (such as collagen and amyloid) motion processes in the lattice. T1 ρ imaging provides a feasible approach to study low-frequency processes, and T1 ρ may detect interstitial fibrosis and other myocardial abnormalities involving large molecules directly [48].

Stress T1 mapping holds promise for assessing coronary microvascular function and vasodilatory reserve in

Fig. 1 Forty-eight-year-old male with myocardial hemochromatosis and history of myelodysplastic syndrome and diabetes mellitus. **a** Cine MR imaging shows dark signal intensity in the myocardium and liver. **b** T2* map shows abnormal value of T2* time (6.5) confirming cardiac hemochromatosis



cardiomyopathies [49]. Compensatory vasodilation in the ischemic myocardium is detectable as mildly increased resting myocardial T1 values, and no change occurs in them during stress because of no further vasodilatory response [50]. Vasodilatory stress and rest T1 mapping may be used to distinguish infarcted, ischemic, and normal myocardium without injection of gadolinium contrast agents. Changes in rest-stress T1 mapping may be used to assess coronary flow reserve in patients with coronary microvascular dysfunction as in diabetic patients without obstructive coronary artery disease [51, 52]. Resting myocardial T1 may mainly reflect the status of the intravascular compartment, rather than only diffuse myocardial fibrosis [49].

Hafmann et al. suggested that in chronic heart failure, impaired exercise capacity is associated with a greater difference between right (RV) to left ventricular (LV) blood pool T2 relaxation times due to a higher level of peripheral blood desaturation compared to healthy controls and patients with preserved exercise capacity [53]. The RV/LV T2 ratio moderately correlated with the percentiles of nominal distances in the 6-min walking test ($r=0.66$), while ejection fraction, end-diastolic, and end-systolic volumes showed no correlation. Additionally, there were significant differences in the RV/LV T2 ratio between patients with and without significant post-exercise dyspnea ($p=0.001$). Regression analyses indicated that the RV/LV T2 ratio was an independent predictor of the distance walked and the presence of post-exercise dyspnea ($p<0.001$).

Four-Dimensional Flow

Four-dimensional flow allows comprehensive evaluation of cardiac and vascular flow. In 4D flow imaging, blood

flow velocity is measured in all three spatial directions and throughout the cardiac cycle. 4D flow has shown its advantages in the evaluation of aortic disease, valvular heart disease, and pulmonary artery disease [54–58] (Fig. 2). A multicenter study showed that valvular flow quantification with automated retrospective valve tracking of 4D flow had a good interobserver agreement and consistency at multiple centers [57].

4D flow gives the opportunity for a comprehensive assessment of hemodynamics including the quantification of flow displacement, wall shear stress, pressure gradients, and turbulent kinetic energy in patients with aortic valvular stenosis [58]. 4D flow may be superior for the quantification of aortic peak velocity and derived pressure gradients, which are important for the assessment of aortic stenosis severity.

4D flow benefits patients with congenital heart diseases such as bicuspid aortic valve or coarctation of the aorta, patients after Fontan palliation, and patients with severe pulmonary valvular regurgitation after surgical repair of tetralogy of Fallot [59]. As for the evaluation of pulmonary regurgitation, 4D flow allows a better quantification of pulmonary regurgitation than 2D flow when taking right ventricle remodeling after pulmonary valve replacement as the reference [60].

Recent CMR technical developments enable more widespread clinical use of 4D flow. They include dual or multi-velocity-encoded cine, respiratory and cardiac self-gating, and accelerated data processing workflows [61].

Diffusion Imaging

Water molecules are constrained by the boundaries in biological tissue, and their diffusion along them shows the

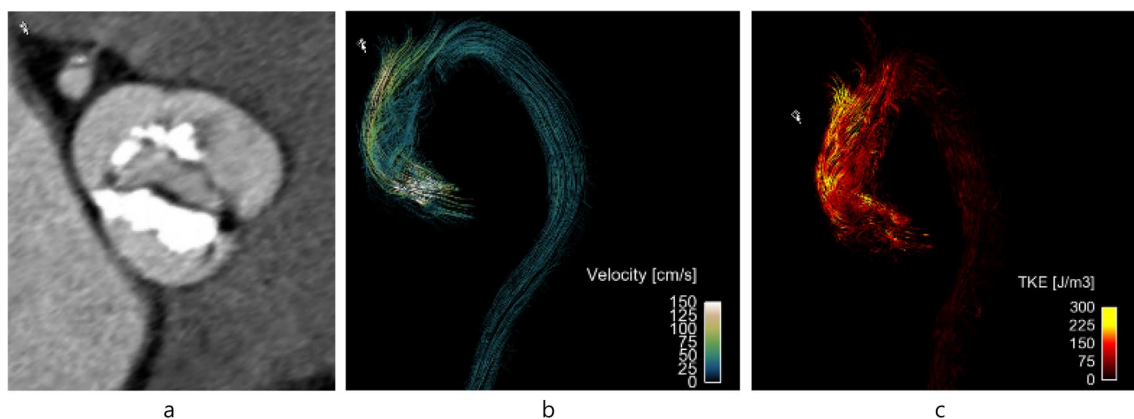


Fig. 2 Four-dimensional MR flow assessment of the ascending aorta in a 73-year-old male with bicuspid aortic valve. CT shows bicuspid AV with calcifications (A). Echocardiography showed mean pressure gradient of 79 mmHg (peak, 132 mmHg) and peak systolic velocity of 5.8 m/s. Flow mapping indicates the streamline of the flow in the ascending aorta (B). Increased velocity and helical flow pattern are

noted in the ascending aorta. The turbulent kinetic energy is visualized by the volume rendering within the entire thoracic aorta (C). The turbulent kinetic energy is increased in the ascending aorta and aortic arch. Images courtesy of Dong Hyun Yang, MD, Asan Medical Center

shape of the myocardial microarchitecture [9]. In vivo assessment of myocardial diffusion is feasible with ongoing advancement in MR techniques, providing new insights on important cardiac pathologies [9]. Further technical developments would improve spatial and angular resolution, scan speed, and scan coverage in cardiac diffusion MR imaging [62].

In acutely infarcted myocardium, diffusion may become more isotropic due to decreased fractional anisotropy. According to Das et al., in patients after ST-elevation myocardial infarction (STEMI), low secondary eigenvector angle values suggested that myocardial sheetlets in acutely infarcted myocardium were unable to adopt their usual steep orientations in systole [63]. The reduction of myocytes with righthanded orientation on helix angle maps was likely reflective of a loss of organization among subendocardial myocytes. Data suggested that the axes of microstructural organization remain relatively fixed after injury. Lower fractal analysis values within acutely infarcted myocardium were independently predictive of poor recovery of LV ejection fraction (standardized $b = 0.57$, $p = 0.008$) [63].

Intravoxel incoherent motion (IVIM) imaging reflects the diffusion parameters of water molecules in tissues and quantitatively describes the signal changes caused by microcirculatory disturbances. IVIM technology enables early and quantitative assessment of microvascular disease in hypertrophic cardiomyopathy (HCM) without contrast agent injection. The proportion of intravoxel microcirculation perfusion effect in the overall diffusion effect, tissue diffusion, and intravoxel microcirculation perfusion-related diffusion movement of the hypertrophic segments and the non-hypertrophic segments were lower than those of the normal group ($p < 0.05$) [16]. The results revealed that the microcirculatory disturbance of HCM existed also in the non-hypertrophic segments with more obvious damage in the hypertrophic segments. Compared with the normal control group, the non-enhanced segments in HCM patients had reduced microcirculatory disturbance and perfusion, and the enhanced segments with more prominent reduction.

Radiomics

Radiomics is a novel research field that aims to identify imaging biomarkers by automated or semi-automated quantitative analysis of medical images. Radiomics analysis on cardiac computed tomography (CT) and magnetic resonance imaging (MRI) images can help identify new imaging biomarkers that may be useful for assessing coronary artery disease, cardiomyopathies, and myocardial viability. Recently, the radiomics quality score (RQS) has been proposed to assess the overall methodological quality of radiomics studies. According to a systemic review, 53 articles on cardiac MRI or CT included in the analysis reached a median total

RQS of 7 (IQR, 4–12), corresponding to a percentage score of 19.4% (IQR, 11.1–33.3%) [64]. To advance radiomics into clinical practice, it is necessary to standardize the radiomics workflow and publication standards for studies.

In the study of Ma et al., a non-contrast T1 mapping-based radiomic nomogram predicted major adverse cardiac events (MACEs) over a period of 1 year in 157 patients with STEMI undergoing percutaneous coronary intervention [65]. The study found that a radiomic signature consisting of three robust features was successful in stratifying patients according to their statistical risk of MACE occurrence. A radiomic nomogram incorporating cTnI levels and radiomic signatures outperformed traditional clinical factors and remote myocardial T1 values in predicting MACE occurrence.

Wang et al. reported that radiomics features derived from late gadolinium-enhanced (LGE) images reflecting myocardial heterogeneity have independent predictive value of sudden cardiac death endpoint in patients with HCM [66].

PET/MRI

A clinical center survey from 47 institutions (18 countries) revealed that 56% of PET/MRI usage was for clinical purposes and that cardiovascular diseases were clinical indications in 17% of PET/MRI [67]. Fluorodeoxyglucose (FDG)-PET/MRI may reclassify non-assessable myocardial segments with intermediate LGE and help diagnose hibernating myocardium [4]. ^{18}F -fluoride may be a marker of high-risk plaques visualized on CMR. In patients with suspected myocarditis, PET and CMR T2 mapping are complimentary with good agreement. In the diagnosis of sarcoidosis, PET/MRI shows areas of active inflammation or fibrosis. PET/MRI can be used to quantify biomarkers of amyloid burden and monitor treatment response. PET/MRI may give additional information in the characterization of cardiac masses.

Strain Imaging

Strain analysis has been used to quantify myocardial deformation in longitudinal, circumferential, and radial directions (Fig. 3). Strain analysis may enable early detection of myocardial dysfunction in the subclinical stages. Myocardial tissue tracking imaging allows for a more accurate evaluation of myocardial deformation beyond the limitations of ejection fraction (EF) [68]. Strain imaging techniques detect and track specific patterns within an image; there are intra- and inter-imaging modality inconsistencies due to imaging modality-related factors such as quality of acquisition process, spatial and temporal resolution, and software-related and operator-related factors [69]. Speckle-tracking echocardiography (STE) has a higher spatial resolution than CMR

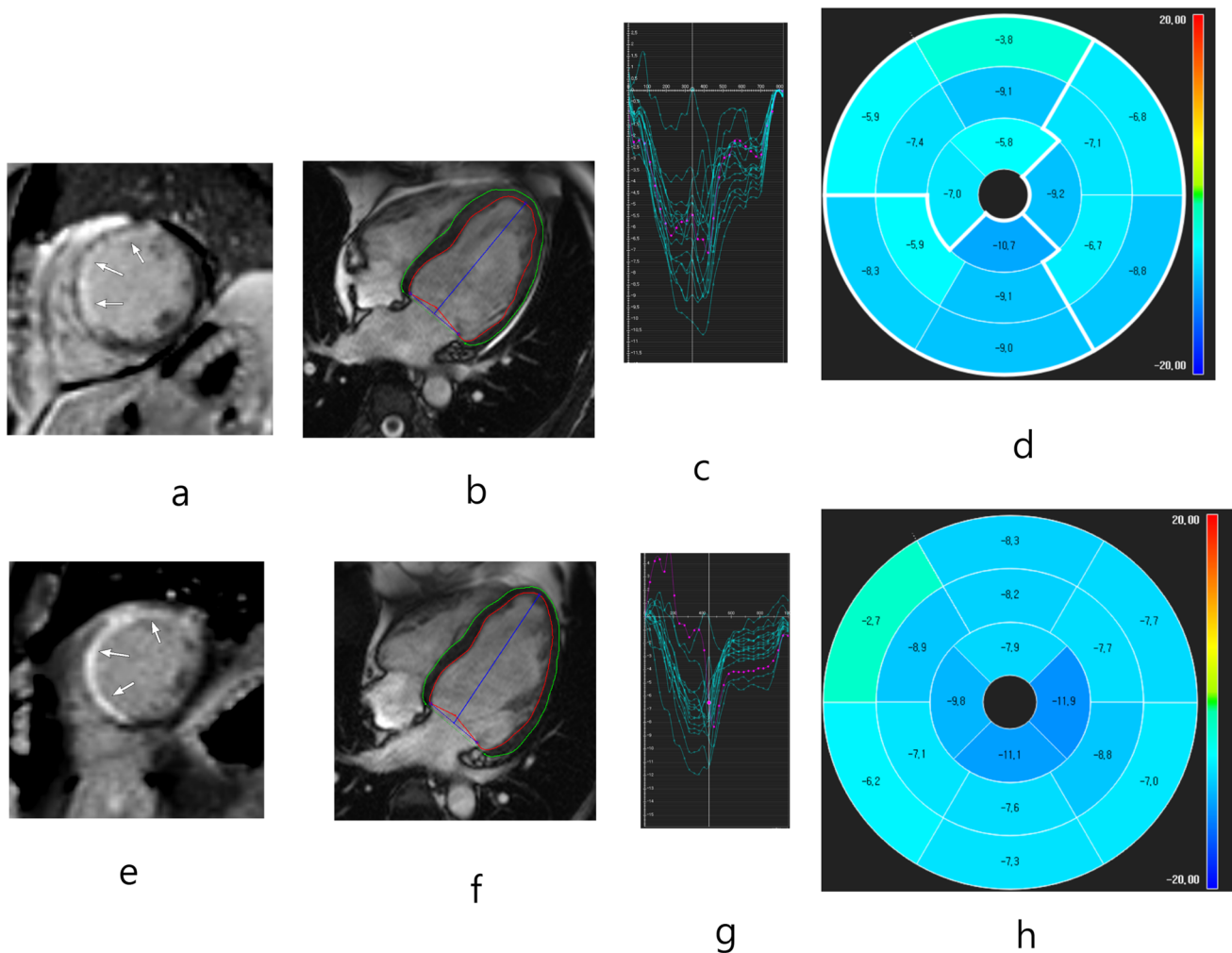


Fig. 3 Forty-four-year-old male with acute myocardial infarction in the territory of left anterior descending branch. Myocardial strain analysis using feature-tracking method (CVI-42) was performed with deep-learning application for the initial (**a**, **b**, **c**, **d**) and 9-month follow-up CMR (**e**, **f**, **g**, **h**). Left ventricular ejection fraction improved from 41.2 to 51.7% and global strain values from 9.19, -9.58 , -4.72

to 14.33, -11.73 , -7.43 for global peak radial, circumferential, and longitudinal strains, respectively. Arrows indicate late gadolinium enhancement in interventricular septum in the initial (**a**) and follow-up studies (**e**). Diagrams and polar map show global longitudinal strains

with a lower signal-to-noise ratio. The echocardiographic images show a lower lateral than axial resolution and lower in-depth resolution [69]. Moreover, the imaging planes of 2D echocardiography might not depict the true apex in long- and short-axis views because of the foreshortening effect. The through-plane motion and foreshortening are overcome by 3D techniques [69]. Similar to STE, segmental deformation assessment with CMR feature tracking (FT) is less reliable than global strain estimation.

Feature tracking (FT) is used to measure strain from routine-balanced steady-state free-precession cine images, while displacement encoding with stimulated echoes (DENSE) provides reliable accuracy and reproducibility comparable to myocardial tagging, the gold standard [70]. Deep learning software, 3D U-Net, named StrainNet, trained by DENSE

data, could be successfully used for strain analysis of conventional cine images in good agreement with DENSE [70].

In a meta-analysis of 44 studies with a total of 3359 healthy subjects, the pooled means of LVGLS, LVGRS, and LVGCS were -18.4% (95% CI: -19.2 to -17.6%), 43.7% (95% CI: 40.0 – 47.4%), and -21.4% (95% CI: -22.3 to -20.6%), respectively [71]. The pooled means of left atrial GLS (total strain, passive strain, and active strain) were 34.9% (95% CI: 29.6 – 40.2%), 21.3% (95% CI: 16.6 – 26.1%), and 14.3% (95% CI: 11.8 – 16.8%), respectively. The pooled means of right ventricular GLS and right atrial total GLS were -24.0% (95% CI: -25.8 to -22.1%) and 36.3% (95% CI: 15.5 – 57.0%), respectively.

According to Oka et al., treatment with sodium-glucose co-transporter 2 inhibitor (SGLT2i) in patients with

diabetes mellitus-related cardiomyopathy showed remarkable improvements in LVGLS (Δ LVGLS: $2.9 \pm 3.0\%$ vs. $0.6 \pm 2.2\%$, $p = 0.005$) and E/e' ($\Delta E/e'$: -1.5 ± 4.7 vs. -0.3 ± 3.0 , $p = 0.253$) compared with controls [72].

In the study of Erley et al. involving 50 patients, there was a good inter-modality agreement between GLS from speckle-tracking echocardiography (STE) and CMR (both feature-tracking [FT] and strain-encoding [SENC]), and the agreement between CMR techniques was better for GLS than GCS [73]. Myocardial strain values derived by both STE and CMR-techniques were highly reproducible, implying values of strain measurements in the follow-up of a patient's disease. In their study group, CMR-derived strain was significantly and independently associated with LGE, whereas STE-GLS was not. This relationship was stronger for GCS than for GLS.

Compressed Sensing

Using single-shot compressed sensing (CS) techniques with sparse sampling and iterative reconstructions, a single cine image can be acquired under free-breathing for a short duration (1 or 2 heartbeats). Single-shot CS cine-derived left ventricular (LV) volumes and myocardial mass measurements correlated strongly with segmented cines ($ICC > 0.798$). However, minor systematic end-systolic volume overestimations resulted in ejection fraction underestimations [74]. In this study, global strains were underestimated in CS cine imaging compared with segmented cine imaging.

In a study of 3.0 T-unenhanced Dixon water-fat whole-heart coronary magnetic resonance angiography (CMRA) using compressed-sensing sensitivity encoding (CS-SENSE) and conventional sensitivity encoding (SENSE), CS-SENSE CMRA had better performance than 2D SENSE regarding the mean acquisition time, signal-to-noise ratio (SNR), and contrast-to-noise ratio (CNR) (7.4 ± 3.2 min vs. 8.3 ± 3.4 min, $p = 0.001$; SNR: 115.5 ± 35.4 vs. 103.3 ± 32.2 ; CNR: 101.1 ± 33.2 vs. 90.6 ± 30.1 , $p < 0.001$ for both) [75].

CS can be applied to 4D flow to accelerate image acquisition [76]. Whole heart 4D flow with conventional parallel imaging (factor 3) as well as CS (factor 7.7) acceleration at 3 T improved acquisition time with CS (6.7 ± 1.3 vs. 12.0 ± 1.3 min). Net forward flow measurements for all valves using conventional and CS acceleration showed good correlation ($r > 0.81$) and agreement ($ICCs > 0.89$). However, CS acceleration underestimated the flow measurements by 3.3–8.3%.

Late Gadolinium Enhancement

LGE images are acquired 8–20 min after intravenous administration of the contrast media (0.1 to 0.2 mmol/kg). Each image data acquisition is preceded by a nonslice-selective

inversion recovery preparation pulse to produce T1-weighted images using sequences such as SSIR-bSSFP or segmented IR-GRE [77]. The inversion recovery (IR) technique enables suppression of the signal from normal myocardial tissue. Careful choice of the time delay (inversion time, TI, typically 300 ms at 1.5 T and 400 ms at 3 T with a contrast dose of 0.15 mmol/kg) after inversion pulse allows the optimization of contrast between tissues and blood [77]. With time-lapse after contrast injection, the optimal TI becomes longer. High TI imaging (TI of around 600 ms at 1.5 T and 875 ms at 3 T) allows differentiation of intracavitary thrombus from enhanced myocardium.

Dark-blood phase-sensitive inversion recovery (PSIR) sequence combining inversion recovery and T2 preparation improves contrast between the scar and nulled signal intensities from both the blood pool and normal myocardium. Dark-blood LGE (FIDDLE) consists of two preparation pulses with a bSSFP readout with phase-sensitive reconstruction [77]. In the study of Si et al., a navigator-gated PSIR sequence provided 3-dimensional high-spatial-resolution ($1.25 \times 1.25 \times 3$ mm³) images in 8.3 min \pm 2.4 (SD) in 20 participants after radiofrequency ablation for atrial fibrillation [78]. The developed PSIR sequence improved the contrast between the atrial scar and blood and achieved a stronger correlation with electroanatomic mapping regarding scar area quantification in comparison with the conventional PSIR sequence.

According to Ohta et al., deviation of inversion time (TI) from the null point can be predicted using a CNN using visual assessment as the reference, and TI correction is also feasible using a smartphone to capture images from the monitor [79]. The results showed that 96.4% of images were corrected to within the optimal range. This suggests that CNN can differentiate changes in tissue contrast from the same cross-sectional image.

Coronary MR Angiography

A recent meta-analysis of 34 studies showed that 1.5 T non-contrast-enhanced whole-heart (WH) CMRA and contrast-enhanced 3.0 T WHCMRA had a summary area under receiver operating characteristic curve (ROC) of 0.88 vs. 0.94 in the patient-based analysis, 0.90 vs. 0.95 in the vessel-based analysis, and 0.92 vs. 0.96 in the segment-based analysis, respectively [80]. On a patient-based analysis, contrast-enhanced 3.0 T WHCMRA had significantly higher specificity than non-contrast-enhanced 1.5 T WHCMRA (0.87, 95% confidence interval [CI] 0.80–0.92 vs. 0.74, 95% CI 0.64–0.82, $p = 0.02$). Regarding the use of vasodilators, beta-blockers or between Asian and Western countries, there were no differences in diagnostic performance on a patient-based analysis.

Ferumoxytol (Feraheme) is a member of the ultrasmall superparamagnetic iron oxide nanoparticles. Ferumoxytol-enhanced CMRA has shown to be effective in detecting coronary stenosis and has an excellent safety profile. According to Dong et al., the sensitivity, specificity, positive predictive value, negative predictive value, and accuracy of ferumoxytol-enhanced CMRA showed 100.0%, 66.7%, 92.3%, 100.0%, and 93.3%, respectively in patient-based analysis; 91.4%, 90.9%, 86.5%, 94.3%, and 91.1%, respectively in vessel-based analysis; and 92.3%, 96.7%, 83.7%, 98.6%, and 96.0%, respectively in segment-based analysis, using the invasive coronary angiography as the reference. No ferumoxytol-related adverse event was observed during the 3-month follow-up [12]. Ferumoxytol-enhanced CMRA emerges as a promising alternative to coronary CT angiography in patients with severe renal insufficiency.

Clinical Applications of CMR: Updates

Amyloidosis

In a meta-analysis, T1 and extracellular volume fraction (ECV) are comparable to LGE for evaluating cardiac amyloidosis (CA) [33]. Only ECV was found to have a significantly better diagnostic and prognostic performance than that of LGE.

Multi-parametric CMR may enable the detection of light-chain amyloidosis with earlier stages. The combination of GCS, GLS, and ECV mapping could distinguish Mayo stage I/II AL amyloidosis from hypertrophic cardiomyopathy with excellent performance (AUC = 0.969, Youden index = 0.813) [81].

Agibetov et al. were able to develop fully automated prediction models for CA using CNN that achieved highly accurate results with average ROC AUC scores ranging from

0.90 to 0.96. The model was validated on a cohort of 502 patients including 82 positive CA patients with endomyocardial biopsy ground-truth labels [82].

Acute Myocarditis

A recent systematic review (53 studies, 2823 myocarditis patients, and 803 controls) showed that LGE has a low sensitivity of 69% and high specificity of 95% for the diagnosis of acute myocarditis, while T1 time had the highest sensitivity (82%), and pericardial effusion had the highest specificity (99%) [83] (Fig. 4). Lake Louise Criteria showed sensitivity of 78% and specificity of 74%. T2 time and ECV showed sensitivities of 75% and 77% and specificities of 84% and 79%, respectively.

LGE has remained in the 2018 updated Lake Louise Criteria due to its high specificity. Detection of myocardial injury with native T1 quantification and detection of edema with T2 weighted imaging or T2 quantification are recommended for the diagnosis of acute myocarditis [34]. Variation in the CMR sequences, symptom onset-to-scan, and the nominal cutoffs used may affect specificity and sensitivity.

Texture analysis applied on CMR T1 and T2 mapping for the diagnosis of acute or chronic myocarditis may be superior to Lake Louise criteria or averaged myocardial T1 or T2 times. In the study of Baessler et al., in 31 participants with acute myocarditis, the combination of mean T2 times and GrayLevelNonUniformity from T2 maps (T2_GLNU) showed the highest area under the curve (AUC) (0.76; 95% confidence interval [CI]: 0.43, 0.95), with sensitivity of 81% and specificity of 71% [84]. In 40 patients with chronic heart failure-like myocarditis, the combination of the two texture features, T2_kurtosis and the GrayLevelNonUniformity from T1, had the highest diagnostic performance (AUC, 0.85; 95% CI: 0.57, 0.90; sensitivity, 90%; and specificity, 72%).

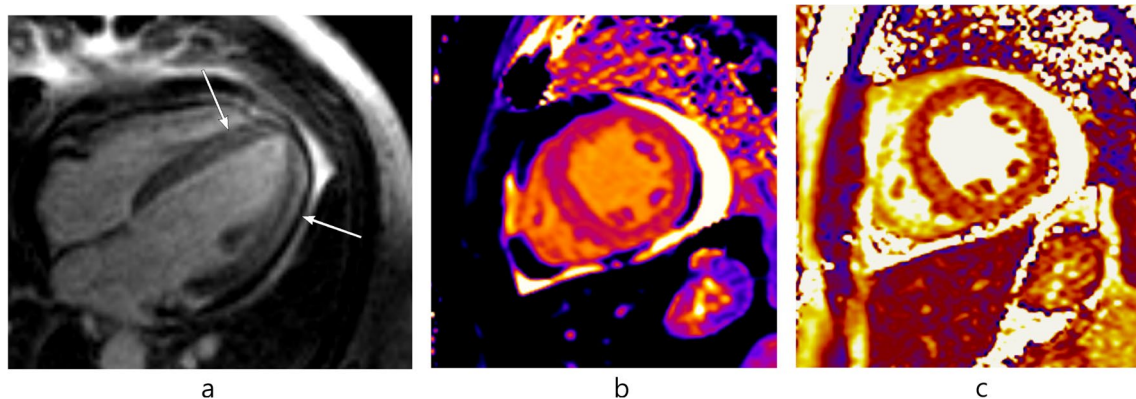


Fig. 4 Thirty-nine-year-old male with lymphocytic myocarditis. **a** Late gadolinium enhancement image shows septal midwall and lateral epicardial enhancement (arrows). **b** native T1 mapping and **c** T2 mapping show elevated values for T1 (1186 ms) and T2 times (78 ms) at 1.5T

Coronavirus Disease (COVID-19) Myopericarditis

In a systemic review of 34 studies on CMR in COVID-19 patients, 21% were normal on CMR [85]. The most common imaging findings were T1 (73%, 109/150) and T2 (63%, 91/144) mapping abnormalities, edema on T2/STIR (51%, 46/90), and LGE (43%, 85/199). Perfusion deficits (85%, 18/21) and extracellular volume mapping abnormalities (52%, 21/40), pericardial effusion (24%, 43/175), and pericardial LGE (22%, 22/100) were also found. LGE was most commonly seen in the subepicardial location (81%) and in the basal-middle inferior segments of the left ventricle. In most patients, ventricular functions were normal.

COVID-19-Vaccine-Related Myocarditis

In a study by Vago et al., a cohort of 16 patients with acute myocarditis (75% mRNA vaccines and 25% vector vaccines) presented with CMR abnormalities depicting myocardial injury, which decreased or completely disappeared on the follow-up visit (mean of 112 days after the acute presentation) [86]. There was an increased T-cell response among myocarditis patients after vaccination compared to matched controls.

A longitudinal study of 5 patients showed normalization of left ventricular ejection fraction in all patients and resolution of myocardial edema in all patients [87]. There was interval improvement of fibrosis seen on LGE, while fibrosis was still present in 80% of patients.

Sarcoidosis

A meta-analysis of eight studies involving 649 patients with histologically proven extra-cardiac sarcoidosis and/or with a suspicion of cardiac sarcoidosis found that cardiac magnetic resonance (CMR) had a pooled sensitivity of 93% and a pooled specificity of 85% for diagnosing cardiac sarcoidosis [88].

Simultaneous cardiac PET/MR detects both inflammation and scar in a single co-registered scan. Cheung et al. have shown that focal fluorodeoxyglucose (FDG) uptake on PET and elevated T2 on MRI had the highest diagnostic specificity among the individual imaging parameters evaluated and are most useful in ruling in cardiac sarcoidosis [89] (Fig. 5). LGE, elevated T1, and elevated ECV had 100% sensitivity. Overall diagnostic performance was the highest for focal FDG uptake accompanied with LGE or elevated T1, highlighting the complementary information provided by combined PET/MRI compared to either modality alone. Combination of focal FDG uptake and LGE was the best predictor of MACE among the imaging findings evaluated.

According to a meta-analysis of 33 studies, CMR may be more sensitive than FDG PET for the detection of cardiac sarcoidosis, with similar specificity. The study found that CMR had higher sensitivity than FDG PET (95% vs 84%, respectively; $p = 0.002$) for the diagnosis of cardiac sarcoidosis, with similar point estimates when the analysis was restricted to studies with direct comparison [90]. According to the study, the specificity of CMR and FDG

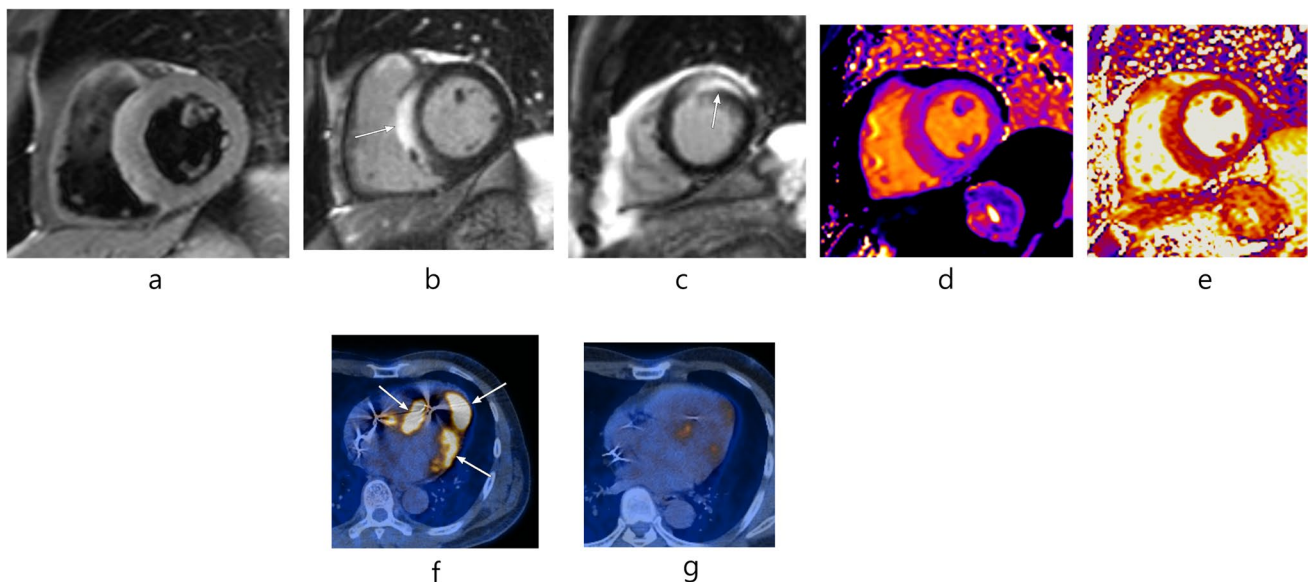


Fig. 5 Fifty-six-year-old male with cardiac sarcoidosis and complete atrioventricular block. **a** T2-weighted image shows mildly increased signal intensity in the basal septum. Late gadolinium enhancement images show strong enhancement (arrows) in basal interventricu-

lar septum (**b**) and mid-anterior wall (**c**). T1 (**d**) and T2 (**e**) mapping shows elevated values for T1 (1174 ms) and T2 times (67 ms) at 1.5T. Initial (**f**) and 3-month (**g**) follow-up FDG-PET CT show improved FDG uptake (arrows) on follow-up after treatment

PET for diagnosing cardiac sarcoidosis did not differ significantly (85% vs 82%, respectively; $p=0.85$). The study found that quantitative evaluation of FDG PET had higher sensitivity than qualitative evaluation (93% vs 76%; $p=0.01$), and inclusion of T2-weighted imaging for MRI had higher sensitivity than exclusion (99% vs 88%; $p=0.001$).

Myocardial Infarction

A meta-analysis revealed that in STEMI patients, the hazard ratio (HR) (95% CI) per 1% increase of myocardial salvage index (MSI) by CMR for cardiac mortality and congestive heart failure was 0.93 (0.91 to 0.96; 1 study, 14/202 events/patients) and 0.96 (0.93 to 0.99; 1 study, 11/104 events/patients), respectively [91].

Persistent microvascular obstruction (MVO) (≥ 1 segment) at follow-up was independently associated with left ventricular end-diastolic index (LVEDVI) and left ventricular end-systolic volume index (LVESVI) [Δ LVEDVI (relative increase, %) ($p<0.001$) and Δ LVESVI ($p<0.001$)] [92].

According to a study, the epicardial surface area (EpiSA) of full-thickness infarction is a novel index of infarct morphology that accurately predicts microvascular obstruction (MVO) during the first 2 weeks of myocardial infarction (MI). Unlike MVO, EpiSA does not disappear with infarct healing [93]. EpiSA extent was associated with adverse ventricular remodeling and worse outcome.

According to a study, cardiac magnetic resonance-tissue tracking-derived myocardial strain after ST-elevation myocardial infarction (STEMI) is related to adverse cardiac events. LVGLS was an independent predictor of LV remodeling [odds ratio (OR) = 1.282, 95% CI = 1.060–1.55, $p=0.011$] with an optimal cut-off of -12.84 (AUC = 0.756, 95% CI = 0.636–0.887, $p<0.001$) [94] (Fig. 1). According to Leung et al., end-systolic (ES) GCS measured with CMR feature tracking was found to be a superior predictor to peak GCS and LGE, after adjusting for pain to balloon time [95].

In patients with reverse left ventricular remodeling (r-LVR) in STEMI, at initial CMR, the r-LVR group had less myocardial damage and higher infarct zone displacement on strain analysis, but there were no differences in global function between the two groups [96]. The infarct zone circumferential and radial strains and radial displacement were higher in the r-LVR group (all $p<0.05$). Microvascular obstruction mass (odds ratio: 0.779 (0.613–0.989), $p=0.041$) and infarct zone peak longitudinal displacement (odds ratio: 1.448 (1.044–2.008), $p=0.026$) were independent predictors of r-LVR.

According to a study, in patients with STEMI, total ischemic time was associated with ECV in infarct areas (ECV_{MI}) but not native T1 in infarct areas ($T1_{MI}$). $T1_{MI}$ improved over time, but the change was not statistically significant among different ischemic time subgroups. ECV_{MI}

was an independent clinical predictor of larger infarct size at 4 months of follow-up [97].

As a promising parameter for early risk stratification after acute myocardial infarction, ECV in acute infarct areas (ECV_{AI}) is associated with LV remodeling during follow-up [35]. The native T1 in acute infarct areas ($T1_{AI}$) did not significantly differ between patients with or without microvascular occlusion (MVO) (1482.0 ± 80.6 ms vs. 1469.0 ± 71.6 ms, $p=0.541$). However, ECV_{AI} in patients without MVO was lower than that in patients with MVO ($49.6 \pm 8.6\%$ vs. $58.5 \pm 8.6\%$, $p=0.001$). The native $T1_{AI}$ only correlated with change in LV end-diastolic volume index (Δ EDV) in patients without MVO ($r=0.495$, $p=0.031$); while ECV_{AI} was associated with Δ EDV in all patients ($r=0.570$, $p<0.001$). Furthermore, ECV_{AI} was independently associated with LV remodeling in multivariable linear regression analysis ($\beta=0.490$, $p=0.002$).

In patients with myocardial infarction with nonobstructive coronary arteries (MINOCA), the %LGE (HR: 1.123 [95% CI: 1.064–1.185]; $p<0.001$) and abnormal T2 times (HR: 1.190 [95% CI: 1.145–1.237]; $p=0.001$) were identified as independent predictors of adverse cardiac events at up to 3.0 years of follow-up [98].

Ischemic Heart Disease

CMR methods for myocardial blood flow (MBF) quantification include tracer-kinetic modeling using blood tissue exchange models, Fermi deconvolution analysis, and model-independent analysis [99]. Myocardial perfusion reserve index (MPRI) can be calculated semi-quantitatively as the stress/rest ratio of myocardial signal intensity upslope. For the upslope-based MPRI, patients with an MPRI < 1.4 showed a high likelihood of having significant microvascular CAD and an MPRI for upslope between 1.4 and 1.6 should encourage further MBF quantification [100].

Three-dimensional (3D) CMR myocardial perfusion imaging may overcome disadvantages of 2-dimensional myocardial perfusion imaging [101]. In a recent multicentric study, 3D CMR perfusion had excellent diagnostic accuracy for the detection of hemodynamically significant lesions, independent of patient age. The sensitivity, specificity, and positive and negative predictive values of 3D CMR perfusion in the detection of hemodynamically relevant (FFR < 0.8) stenosis were similar in age groups ≥ 75 years and < 75 years [102].

Stress perfusion CMR was statistically superior to gated single-photon emission computed tomography (SPECT) for specificity ($p=0.002$), area under the receiver operating characteristic curve ($p<0.001$), accuracy ($p=0.003$), positive predictive value ($p<0.001$), and negative predictive value ($p=0.041$). The sensitivity of

CMR for a 70% quantitative coronary angiography stenosis was noninferior and nonsuperior to gated SPECT [103].

As for the differentiation of ischemic (IC) from nonischemic cardiomyopathy (NIC), in the study of Wang et al., MPRI using stress perfusion CMR was not different between IC and NIC [104]. However, in patients with NIC, MPRI was correlated with LVEF, although this relation was not seen in patients with IC.

Perfusion CMR is regarded as a well-validated gatekeeper for invasive angiography with strengths across the whole spectrum of pre-test likelihoods [105]. In the MR-INFORM study, the subsequent management of patients with intermediate-to-high pretest likelihoods could be decided safely based on perfusion CMR and that perfusion CMR was non-inferior to invasive angiography supported by fractional flow reserve (FFR) [106] (Fig. 6).

In the CMR-IMPACT trial (Cardiac Magnetic Resonance Imaging Strategy for the Management of Patients with Acute Chest Pain and Detectable to Elevated Troponin), 312 participants with acute chest pain symptoms and a contemporary troponin between detectable and 1.0 ng/mL were randomized early in their care to invasive-based ($n = 156$) or CMR-based ($n = 156$) management [107]. Among patients completing CMR imaging, 55 out of 95 (58%) were safely identified for discharge based on a negative CMR and did not have angiography or revascularization within 90 days. The therapeutic yield of angiography was higher in the CMR-based arm (52 interventions in 81 angiographies [64.2%]) compared to the invasive-based arm (46 interventions in 115 angiographies [40.0%]).

Hypertrophic Cardiomyopathy

According to the 2020 AHA/ACC Guideline for the Diagnosis and Treatment of Patients With Hypertrophic Cardiomyopathy, CMR imaging will be helpful in patients, in whom there is diagnostic uncertainty, poor echocardiographic imaging windows, or where uncertainty persists regarding decisions around implantable cardioverter-defibrillator (ICD) placement [108]. CMR is regarded beneficial to assess the risks for sudden death such as maximum left ventricular wall thickness (≥ 30 mm or Z score ≥ 20), ejection fraction ($< 50\%$), LV apical aneurysm, and extent of myocardial fibrosis ($> 15\%$ of LV mass). CMR is indicated to inform the selection and planning of septal reduction therapy for patients with obstructive HCM with inconclusive echocardiographic information. Periodic (every 3 to 5 years) LGE CMR may be considered to assess the risk of sudden cardiac death (Fig. 7).

Freitas et al. compared the prognostic value of the amount of LGE with the two currently recommended risk stratification tools in an HCM population [109]. The amount of LGE was the only independent predictor of outcome (adjusted HR: 1.08; 95% CI: 1.04–1.12; $p < 0.001$) after adjustment for the HCM Risk-sudden cardiac death (SCD) and ACCF/AHA criteria. The amount of LGE showed greater discriminative power (C-statistic 0.84; 95% CI: 0.76–0.91) than the ACCF/AHA criteria (C-statistic 0.61; 95% CI: 0.49–0.72; p for comparison < 0.001) and the HCM Risk-SCD (C-statistic 0.68; 95% CI: 0.59–0.78; p for comparison = 0.006). LGE could increase the discriminative power of the ACCF/AHA and HCM Risk-SCD criteria, with net reclassification improvements of 0.36 ($p = 0.021$) and 0.43 ($p = 0.011$), respectively.

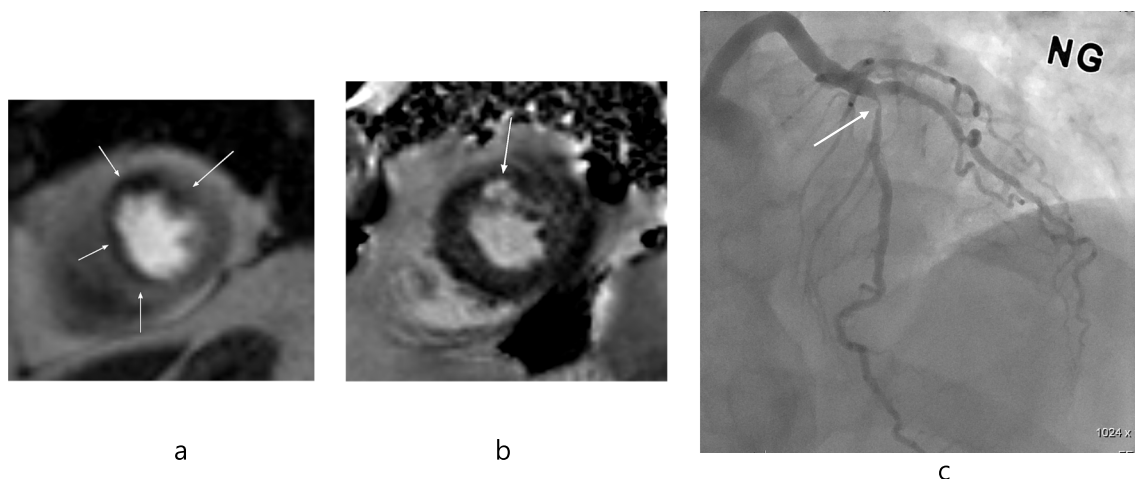
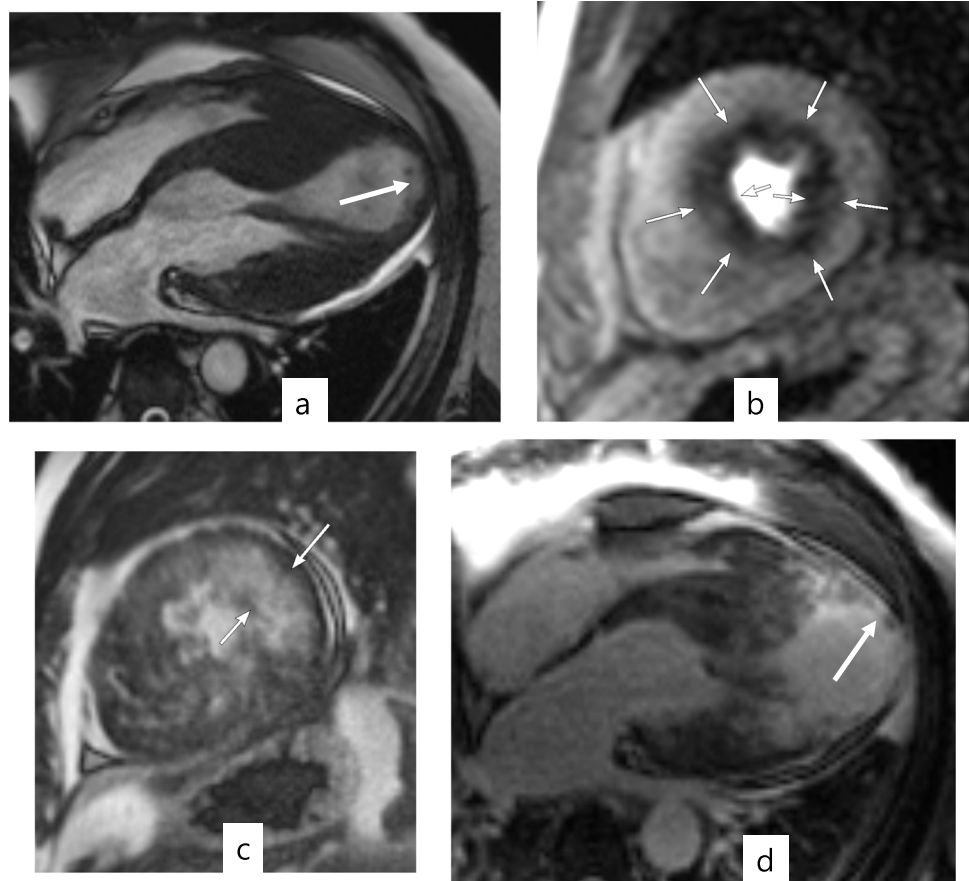


Fig. 6 Seventy-two-year-old male with myocardial ischemia. **a** Adenosine stress perfusion MRI shows perfusion defects (arrows) in mid-septal and anterior walls. **b** Late gadolinium enhancement image

shows focal area of subendocardial enhancement (arrow) due to old myocardial infarction. **c** Coronary angiography visualizes severe stenosis (arrow) in mid-left anterior descending branch

Fig. 7 Fifty-eight-year-old male with hypertrophic cardiomyopathy. **a** Systolic cine image show apical aneurysm (arrow) with mid-ventricular obstruction. **b** Adenosine stress perfusion MRI shows circumferential perfusion defects (arrows) in mid-ventricular segments. **c** and **d** Late gadolinium enhancement images show myocardial fibrosis (arrows)



Suwa et al. reported that 4D flow can be used to assess the success of alcohol septal ablation showing flow pathway and acceleration at the mid-ventricle [110]. The reduction in flow velocity at the mid-ventricle after alcohol septal ablation suggested the relief of mid-ventricular obstruction.

Dilated Cardiomyopathy

Becker et al. aimed to assess the importance of septal mid-wall LGE in patients with dilated cardiomyopathy (DCM) [111]. Septal midwall LGE was seen in 55 patients with ischemic cardiomyopathy (ICM) (10%) and in 172 patients (34%) with DCM. During follow-up, the presence of septal midwall LGE was significantly associated with increased all-cause mortality in patients with DCM but not in patients with ischemic cardiomyopathy. The presence of septal mid-wall LGE was also significantly associated with the composite secondary ventricular arrhythmic endpoint, regardless of the underlying etiology.

In a study of 417 patients with DCM, the 16-segment standard deviation of the time-to-peak radial strain (HR, 1.932 [95% CI: 1.079, 3.461]; $p=0.027$), LV end-diastolic diameter index (HR, 1.049 [95% CI: 1.020, 1.080]; $p=0.001$), NYHA classes (HR, 2.131 [95% CI:

1.597–2.844]; $p<0.001$), and LGE (HR, 3.219 [95% CI: 2.164, 4.787]; $p<0.001$) were independently associated with composite endpoints (19, sudden cardiac death; 34, heart failure death; 41, heart transplantation; 9, malignant ventricular arrhythmias; 2, LV assist devices; and 4, appropriate shocks of defibrillators) [112].

In the study of Liu et al., a new marker of CMR LV global function index (LVGFI), $[\text{LV stroke volume}/(\text{LV end-diastolic volume} + \text{LV end-systolic volume})/2] \times 100\%$, was 16.5% in 334 DCM patients [113]. The long-term risk of the composite endpoint in patients with DCM over a median follow-up period of 565 days was significantly negatively associated with CMR-LVGFI. For every 1 SD increase in CMR-LVGFI, an HR of the composite endpoint after adjusting the clinical, laboratory, electrocardiogram, and CMR routine variables decreased by 46%, which was evident in all the subgroups after adjustments.

Concomitant hypertension further deteriorated LV global longitudinal peak strain (PS) and peak diastolic strain rate (PDSR) in patients with DCM [114]. The LV remodeling index was significantly increased, and the presence of LGE was higher in DCM patients with hypertension than in those without hypertension; after adjustment for confounding factors, hypertension was found to be an independent

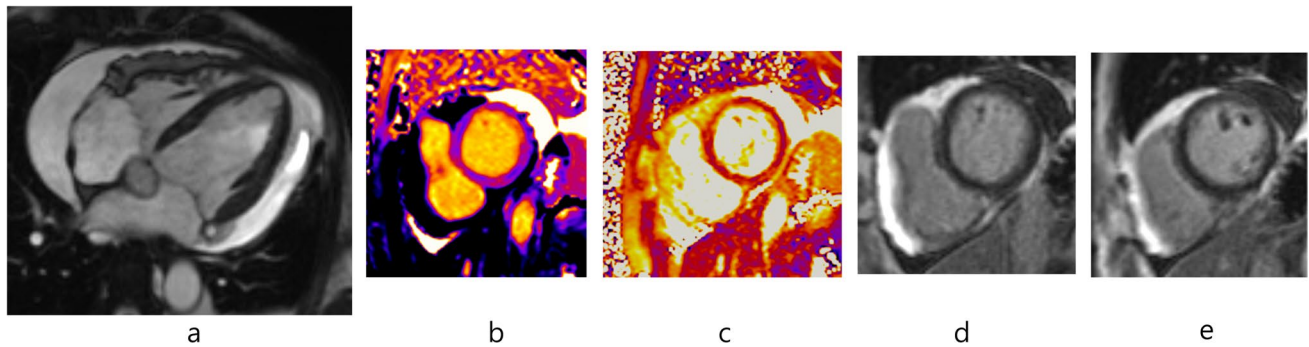


Fig. 8 Forty-eight-year-old female with breast cancer and chemotherapy-induced cardiomyopathy. Cine image shows pericardial effusion. Global left ventricular ejection fraction was 42% (a). T1 (b) and T2 (c) mapping show elevated values for T1 (1049 ms) and T2 times

(64 ms) at 1.5T. Extracellular volume fraction measured 33.8%. Late gadolinium enhancement images show no abnormal enhancement (d) except a basal septal stripe (e)

determinant of reduced LV global longitudinal PS and PDSR, and systolic and diastolic blood pressure were independent determinants of the LV remodeling index in patients with DCM.

Cardiotoxicity After Chemotherapy

Anthracyclines are thought to cause excess collagen deposition [115]. Several studies showed elevated myocardial T1 and ECV in patients treated with anthracyclines compared with age- and sex-matched controls (Fig. 8). In an animal study of anthracycline-induced cardiotoxicity, T2 mapping abnormalities provided the earliest marker of subtle myocardial damage, with T2 relaxation times prolonged long before LV motion abnormalities were detected, while T1 relaxation times and ECV quantification were not changed [116]. Pathology evaluation revealed an absolute increase in myocardial water content, correlating with vacuole formation in preserved cardiomyocytes but with no concomitant fibrosis or increased extracellular space.

T1 and T2 mapping techniques are also useful for the diagnosis and monitoring of myocarditis, which has been associated with various cancer agents, with increasing recognition [117]. CMR is especially useful in monitoring cardiac function throughout treatment with potentially cardiotoxic chemotherapy [118].

Reimbursement and Cost-Effectiveness in Cardiac MR

The CMR test is relatively expensive in Korea. The Ministry of Health and Welfare of Korea has covered the fees in part for CMR examinations in patients with cardiomyopathy, complex congenital heart diseases, and anomalies of the great vessels since November 2019 [119]. In the USA and Australia, stress CMR is cost-effective for patients for

the diagnosis of significant coronary artery disease [120, 121]. In The STRATEGY Study comparing coronary CT angiography (CCTA) and stress CMR, patients undergoing stress CMR showed a lower rate of major adverse cardiac events and cost-effectiveness ratio [122]. In an outcome-based study, CMR results helped avoid invasive procedures in 11% of patients and prevented additional diagnostic studies in 7% with cost savings [123].

Conclusion

Recent developments in CMR incorporating AI enable faster image acquisition and automated image analysis. Myocardial parametric mapping, strain analysis of cardiac chambers, and 4D flow give new insights on cardiovascular diseases with widened applications of CMR than before.

Author Contributions Conceptualization: Yeon Hyeon Choe and Sung Mok Kim; writing—original draft: Yeon Hyeon Choe; writing—review and editing: Yeon Hyeon Choe and Sung Mok Kim.

Data Availability Not applicable.

Declarations

Conflict of Interest Yeon Hyeon Choe and Sung Mok Kim declare that they have no conflict of interest.

Ethics Approval All content in this editorial was in accordance with the ethical standards of the institutional and/or national research committee and with the 1964 Helsinki Declaration and its later amendments or comparable ethical standards.

Consent to Participate As an editorial article obtaining informed consent was waived.

Consent for Publication Not applicable.

References

- Busse A, Rajagopal R, Yücel S, Beller E, Öner A, Streckenbach F, et al. Cardiac MRI-update 2020. *Radiologe*. 2020;60(Suppl 1):33–40. <https://doi.org/10.1007/s00117-020-00687-1>.
- Daubert MA, Taylor T, James O, Shaw LJ, Douglas PS, Koweek L. Multimodality cardiac imaging in the 21st century: evolution, advances and future opportunities for innovation. *Br J Radiol*. 2021;94(1117):20200780. <https://doi.org/10.1259/bjr.20200780>.
- Dodd JD, Leipsic J. Cardiovascular CT and MRI in 2019: review of key articles. *Radiology*. 2020;297(1):17–30. <https://doi.org/10.1148/radiol.20200605>.
- Chowdhary A, Garg P, Das A, Nazir MS, Plein S. Cardiovascular magnetic resonance imaging: emerging techniques and applications. *Heart*. 2021. <https://doi.org/10.1136/heartjnl-2019-315669>.
- Eck BL, Flamm SD, Kwon DH, Tang WHW, Vasquez CP, Seiberlich N. Cardiac magnetic resonance fingerprinting: trends in technical development and potential clinical applications. *Prog Nucl Magn Reson Spectrosc*. 2021;122:11–22. <https://doi.org/10.1016/j.pnmrs.2020.10.001>.
- Seraphim A, Knott KD, Augusto J, Bhuvana AN, Manisty C, Moon JC. Quantitative cardiac MRI. *J Magn Reson Imaging*. 2020;51(3):693–711. <https://doi.org/10.1002/jmri.26789>.
- Tang F, Bai C, Zhao XX, Yuan WF. Artificial intelligence and myocardial contrast enhancement pattern. *Curr Cardiol Rep*. 2020;22(8):77. <https://doi.org/10.1007/s11886-020-01306-0>.
- Velasco C, Fletcher TJ, Botnar RM, Prieto C. Artificial intelligence in cardiac magnetic resonance fingerprinting. *Front Cardiovasc Med*. 2022;9:1009131. <https://doi.org/10.3389/fcvm.2022.1009131>.
- Nielles-Vallespin S, Scott A, Ferreira P, Khaliq Z, Pennell D, Firmin D. Cardiac diffusion: technique and practical applications. *J Magn Reson Imaging*. 2020;52(2):348–68. <https://doi.org/10.1002/jmri.26912>.
- Liu Y, Hamilton J, Jiang Y, Seiberlich N. Cardiac MRF using rosette trajectories for simultaneous myocardial T(1), T(2), and proton density fat fraction mapping. *Front Cardiovasc Med*. 2022;9: 977603. <https://doi.org/10.3389/fcvm.2022.977603>.
- Weingärtner S, Demirel ÖB, Gama F, Pierce I, Treibel TA, Schulz-Menger J, et al. Cardiac phase-resolved late gadolinium enhancement imaging. *Front Cardiovasc Med*. 2022;9: 917180. <https://doi.org/10.3389/fcvm.2022.917180>.
- Dong Z, Si G, Zhu X, Li C, Hua R, Teng J, et al. Diagnostic performance and safety of a novel ferumoxytol-enhanced coronary magnetic resonance angiography. *Circ Cardiovasc Imaging*. 2023;16(7):580–90. <https://doi.org/10.1161/circimaging.123.015404>.
- Ayala C, Luo H, Godines K, Alghuraibawi W, Ahn S, Rehwald W, et al. Individually tailored spatial-spectral pulsed CEST MRI for ratiometric mapping of myocardial energetic species at 3T. *Magn Reson Med*. 2023. <https://doi.org/10.1002/mrm.29801>.
- Buechel RR, Ciancone D, Bakula A, von Felten E, Schmidt GA, Patriki D, et al. Long-term impact of myocardial inflammation on quantitative myocardial perfusion—a descriptive PET/MR myocarditis study. *Eur J Nucl Med Mol Imaging*. 2023. <https://doi.org/10.1007/s00259-023-06314-0>.
- Bakermans AJ, Boekholdt SM, de Vries DK, Reckman YJ, Farag ES, de Heer P, et al. Quantification of myocardial creatine and triglyceride content in the human heart: precision and accuracy of in vivo proton magnetic resonance spectroscopy. *J Magn Reson Imaging*. 2021. <https://doi.org/10.1002/jmri.27531>.
- Abulaiti A, Zhang Q, Huang H, Ding S, Shayiti M, Wang S, et al. The value of the cardiac magnetic resonance intravoxel incoherent motion technique in evaluating microcirculatory dysfunction in hypertrophic cardiomyopathy. *J Interv Cardiol*. 2023;2023:4611602. <https://doi.org/10.1155/2023/4611602>.
- Lara Hernandez KA, Rienmüller T, Baumgartner D, Baumgartner C. Deep learning in spatiotemporal cardiac imaging: a review of methodologies and clinical usability. *Comput Biol Med*. 2021;130: 104200. <https://doi.org/10.1016/j.combiomed.2020.104200>.
- Alskaf E, Dutta U, Scannell CM, Chiribiri A. Deep learning applications in myocardial perfusion imaging, a systematic review and meta-analysis. *Inform Med Unlocked*. 2022;32: 101055. <https://doi.org/10.1016/j.imu.2022.101055>.
- Wang ZC, Fan ZZ, Liu XY, Zhu MJ, Jiang SS, Tian S, et al. Deep learning for discrimination of hypertrophic cardiomyopathy and hypertensive heart disease on MRI native T1 Maps. *J Magn Reson Imaging*. 2023. <https://doi.org/10.1002/jmri.28904>.
- Chen BH, Wu CW, An DA, Zhang JL, Zhang YH, Yu LZ, et al. A deep learning method for the automated assessment of paradoxical pulsation after myocardial infarction using multicenter cardiac MRI data. *Eur Radiol*. 2023. <https://doi.org/10.1007/s00330-023-09807-6>.
- Kim YC, Kim KR, Choe YH. Automatic myocardial segmentation in dynamic contrast enhanced perfusion MRI using Monte Carlo dropout in an encoder-decoder convolutional neural network. *Comput Methods Programs Biomed*. 2020;185: 105150. <https://doi.org/10.1016/j.cmpb.2019.105150>.
- Kim YC, Kim KR, Choi K, Kim M, Chung Y, Choe YH. EVCMR: a tool for the quantitative evaluation and visualization of cardiac MRI data. *Comput Biol Med*. 2019;111: 103334. <https://doi.org/10.1016/j.combiomed.2019.103334>.
- Xu B, Kocyigit D, Grimm R, Griffin BP, Cheng F. Applications of artificial intelligence in multimodality cardiovascular imaging: a state-of-the-art review. *Prog Cardiovasc Dis*. 2020;63(3):367–76. <https://doi.org/10.1016/j.pcad.2020.03.003>.
- Fan L, Shen D, Haji-Valizadeh H, Naresh NK, Carr JC, Freed BH, et al. Rapid dealiasing of undersampled, non-Cartesian cardiac perfusion images using U-net. *NMR Biomed*. 2020;33(5): e4239. <https://doi.org/10.1002/nbm.4239>.
- Unal HB, Beaulieu T, Rivero LZ, Dharmakumar R, Sharif B. Retrospective detection and suppression of dark-rim artifacts in first-pass perfusion cardiac MRI enabled by deep learning. *Annu Int Conf IEEE Eng Med Biol Soc*. 2021;2021:4079–85. <https://doi.org/10.1109/embc46164.2021.9630270>.
- Yan X, Luo Y, Chen X, Chen EZ, Liu Q, Zou L, et al. From compressed-sensing to deep learning MR: comparative biventricular cardiac function analysis in a patient cohort. *J Magn Reson Imaging*. 2023. <https://doi.org/10.1002/jmri.28899>.
- Küstner T, Armanious K, Yang J, Yang B, Schick F, Gatidis S. Retrospective correction of motion-affected MR images using deep learning frameworks. *Magn Reson Med*. 2019;82(4):1527–40. <https://doi.org/10.1002/mrm.27783>.
- Fahmy AS, Rowin EJ, Chan RH, Manning WJ, Maron MS, Nezafat R. Improved quantification of myocardium scar in late gadolinium enhancement images: deep learning based image fusion approach. *J Magn Reson Imaging*. 2021. <https://doi.org/10.1002/jmri.27555>.
- Zabihollahy F, Rajan S, Ukwatta E. Machine learning-based segmentation of left ventricular myocardial fibrosis from magnetic resonance imaging. *Curr Cardiol Rep*. 2020;22(8):65. <https://doi.org/10.1007/s11886-020-01321-1>.
- Gao Y, Zhou Z, Zhang B, Guo S, Bo K, Li S, et al. Deep learning-based prognostic model using non-enhanced cardiac cine MRI for outcome prediction in patients with heart failure. *Eur Radiol*. 2023. <https://doi.org/10.1007/s00330-023-09785-9>.
- Moustafa A, Khan MS, Alsamman MA, Jamal F, Atalay MK. Prognostic significance of T1 mapping parameters in heart

- failure with preserved ejection fraction: a systematic review. *Heart Fail Rev.* 2021;26(6):1325–31. <https://doi.org/10.1007/s10741-020-09958-4>.
32. Pan C, Zhang Z, Luo L, Wu W, Jia T, Lu L, et al. Cardiac T1 and T2 mapping showed myocardial involvement in recovered COVID-19 patients initially considered devoid of cardiac damage. *J Magn Reson Imaging.* 2021. <https://doi.org/10.1002/jmri.27534>.
 33. Pan JA, Kerwin MJ, Salerno M. Native T1 Mapping, extracellular volume mapping, and late gadolinium enhancement in cardiac amyloidosis: a meta-analysis. *JACC Cardiovasc Imaging.* 2020;13(6):1299–310. <https://doi.org/10.1016/j.jcmg.2020.03.010>.
 34. When P, Armstrong R, Daly CA. Recent advances in T1 and T2 mapping in the assessment of fulminant myocarditis by cardiac magnetic resonance. *Curr Cardiol Rep.* 2020;22(7):47. <https://doi.org/10.1007/s11886-020-01295-0>.
 35. Yang MX, He Y, Ma M, Zhao Q, Xu HY, Xia CC, et al. Characterization of infarcted myocardium by T1-mapping and its association with left ventricular remodeling. *Eur J Radiol.* 2021;137:109590. <https://doi.org/10.1016/j.ejrad.2021.109590>.
 36. Yue P, Xu Z, Wan K, Tan Y, Xu Y, Xie X, et al. Multiparametric mapping by cardiovascular magnetic resonance imaging in cardiac tumors. *J Cardiovasc Magn Reson.* 2023;25(1):37. <https://doi.org/10.1186/s12968-023-00938-9>.
 37. Roller FC, Fuest S, Meyer M, Harth S, Gündüz D, Bauer P, et al. Assessment of cardiac involvement in Fabry Disease (FD) with native T1 mapping. *Rofo.* 2019;191(10):932–9. <https://doi.org/10.1055/a-0836-2723>.
 38. Krittayaphong R, Zhang S, Saiviroonporn P, Viprakasit V, Tanapibunpon P, Komoltri C, et al. Detection of cardiac iron overload with native magnetic resonance T1 and T2 mapping in patients with thalassemia. *Int J Cardiol.* 2017;248:421–6. <https://doi.org/10.1016/j.ijcard.2017.06.100>.
 39. Ferreira VM, Piechnik SK. CMR Parametric mapping as a tool for myocardial tissue characterization. *Korean Circ J.* 2020;50(8):658–76. <https://doi.org/10.4070/kcj.2020.0157>.
 40. Shin SH, Kim SM, Cho SJ, Choe YH. Longitudinal changes in the myocardial T1 relaxation time, extracellular volume fraction, and left ventricular function in asymptomatic men. *J Cardiovasc Dev Dis.* 2023;10(6). <https://doi.org/10.3390/jcdd10060252>.
 41. Warnica W, Al-Arnawoot A, Stanimirovic A, Thavendirathan P, Wald RM, Pakkal M, et al. Clinical Impact of Cardiac MRI T1 and T2 Parametric mapping in patients with suspected cardiomyopathy. *Radiology.* 2022;305(2):319–26. <https://doi.org/10.1148/radiol.220067>.
 42. Messroghli DR, Moon JC, Ferreira VM, Grosse-Wortmann L, He T, Kellman P, et al. Clinical recommendations for cardiovascular magnetic resonance mapping of T1, T2, T2* and extracellular volume: a consensus statement by the Society for Cardiovascular Magnetic Resonance (SCMR) endorsed by the European Association for Cardiovascular Imaging (EACVI). *J Cardiovasc Magn Reson.* 2017;19(1):75. <https://doi.org/10.1186/s12968-017-0389-8>.
 43. Ferreira VM, Schulz-Menger J, Holmvang G, Kramer CM, Carbone I, Sechtem U, et al. Cardiovascular magnetic resonance in nonischemic myocardial inflammation: expert recommendations. *J Am Coll Cardiol.* 2018;72(24):3158–76. <https://doi.org/10.1016/j.jacc.2018.09.072>.
 44. Kalapos A, Szabó L, Dohy Z, Kiss M, Merkely B, Gyires-Tóth B, et al. Automated T1 and T2 mapping segmentation on cardiovascular magnetic resonance imaging using deep learning. *Front Cardiovasc Med.* 2023;10:1147581. <https://doi.org/10.3389/fcvm.2023.1147581>.
 45. Kim YC, Kim KR, Lee H, Choe YH. Fast calculation software for modified Look-Locker inversion recovery (MOLLI) T1 mapping. *BMC Med Imaging.* 2021;21(1):26. <https://doi.org/10.1186/s12880-021-00558-8>.
 46. Qi H, Lv Z, Hu J, Xu J, Botnar R, Prieto C, et al. Accelerated 3D free-breathing high-resolution myocardial T(1ρ) mapping at 3 Tesla. *Magn Reson Med.* 2022;88(6):2520–31. <https://doi.org/10.1002/mrm.29417>.
 47. Si D, Kong X, Guo R, Cheng L, Ning Z, Chen Z, et al. Single breath-hold three-dimensional whole-heart T(2) mapping with low-rank plus sparse reconstruction. *NMR Biomed.* 2023;36(8):e4924. <https://doi.org/10.1002/nbm.4924>.
 48. Bustin A, Witschey WRT, van Heeswijk RB, Cochet H, Stuber M. Magnetic resonance myocardial T1ρ mapping : technical overview, challenges, emerging developments, and clinical applications. *J Cardiovasc Magn Reson.* 2023;25(1):34. <https://doi.org/10.1186/s12968-023-00940-1>.
 49. Piechnik SK, Neubauer S, Ferreira VM. State-of-the-art review: stress T1 mapping-technical considerations, pitfalls and emerging clinical applications. *MAGMA.* 2018;31(1):131–41. <https://doi.org/10.1007/s10334-017-0649-5>.
 50. Liu A, Wijesurendra RS, Francis JM, Robson MD, Neubauer S, Piechnik SK, et al. Adenosine stress and rest T1 mapping can differentiate between ischemic, infarcted, remote, and normal myocardium without the need for gadolinium contrast agents. *JACC Cardiovasc Imaging.* 2016;9(1):27–36. <https://doi.org/10.1016/j.jcmg.2015.08.018>.
 51. Ma P, Liu J, Hu Y, Zhou X, Shang Y, Wang J. Histologic validation of stress cardiac magnetic resonance T1-mapping techniques for detection of coronary microvascular dysfunction in rabbits. *Int J Cardiol.* 2022;347:76–82. <https://doi.org/10.1016/j.ijcard.2021.10.137>.
 52. Ma P, Liu J, Hu Y, Chen L, Liang H, Zhou X, et al. Stress CMR T1-mapping technique for assessment of coronary microvascular dysfunction in a rabbit model of type II diabetes mellitus: Validation against histopathologic changes. *Front Cardiovasc Med.* 2022;9:1066332. <https://doi.org/10.3389/fcvm.2022.1066332>.
 53. Halfmann MC, Müller L, von Henning U, Kloeckner R, Schöler T, Kreitner KF, et al. Cardiac MRI-based right-to-left ventricular blood pool T2 relaxation times ratio correlates with exercise capacity in patients with chronic heart failure. *J Cardiovasc Magn Reson.* 2023;25(1):33. <https://doi.org/10.1186/s12968-023-00943-y>.
 54. Rizk J. 4D flow MRI applications in congenital heart disease. *Eur Radiol.* 2021;31(2):1160–74. <https://doi.org/10.1007/s00330-020-07210-z>.
 55. Jamaludin F, Hassanabad AF, François CJ, Garcia J. Four-dimensional-flow magnetic resonance imaging of the aortic valve and thoracic aorta. *Radiol Clin North Am.* 2020;58(4):753–63. <https://doi.org/10.1016/j.rcl.2020.02.008>.
 56. Corrias G, Cocco D, Suri JS, Meloni L, Cademartiri F, Saba L. Heart applications of 4D flow. *Cardiovasc Diagn Ther.* 2020;10(4):1140–9. <https://doi.org/10.21037/cdt.2020.02.08>.
 57. Juffermans JF, Minderhoud SCS, Wittgren J, Kilburg A, Ese A, Fidock B, et al. Multicenter consistency assessment of valvular flow quantification with automated valve tracking in 4D flow CMR. *JACC Cardiovasc Imaging.* 2021. <https://doi.org/10.1016/j.jcmg.2020.12.014>.
 58. Garcia J, Barker AJ, Markl M. The role of imaging of flow patterns by 4D flow MRI in aortic stenosis. *JACC Cardiovasc Imaging.* 2019;12(2):252–66. <https://doi.org/10.1016/j.jcmg.2018.10.034>.
 59. Warmerdam E, Krings GJ, Leiner T, Grotenhuis HB. Three-dimensional and four-dimensional flow assessment in congenital heart disease. *Heart.* 2020;106(6):421–6. <https://doi.org/10.1136/heartjnl-2019-315797>.
 60. Soulat G, Alattar Y, Ladouceur M, Craiem D, Pascaner A, Gencer U, et al. Discordance between 2D and 4D flow in the

- assessment of pulmonary regurgitation severity: a right ventricular remodeling follow-up study. *Eur Radiol.* 2023;33(8):5455–64. <https://doi.org/10.1007/s00330-023-09502-6>.
61. Bissell MM, Raimondi F, Ait Ali L, Allen BD, Barker AJ, Bolger A, et al. 4D Flow cardiovascular magnetic resonance consensus statement: 2023 update. *J Cardiovasc Magn Reson.* 2023;25(1):40. <https://doi.org/10.1186/s12968-023-00942-z>.
 62. Khalique Z, Ferreira PF, Scott AD, Nielles-Vallespin S, Firmin DN, Pennell DJ. Diffusion tensor cardiovascular magnetic resonance imaging: a clinical perspective. *JACC Cardiovasc Imaging.* 2020;13(5):1235–55. <https://doi.org/10.1016/j.jcmg.2019.07.016>.
 63. Das A, Kelly C, Teh I, Stoeck CT, Kozerke S, Chowdhary A et al. Acute microstructural changes after ST-segment elevation myocardial infarction assessed with diffusion tensor imaging. *Radiology.* 2021;203208. <https://doi.org/10.1148/radiol.2021203208>.
 64. Ponsiglione A, Stanzione A, Cuocolo R, Ascione R, Gambardella M, De Giorgi M, et al. Cardiac CT and MRI radiomics: systematic review of the literature and radiomics quality score assessment. *Eur Radiol.* 2022;32(4):2629–38. <https://doi.org/10.1007/s00330-021-08375-x>.
 65. Ma Q, Ma Y, Wang X, Li S, Yu T, Duan W, et al. A radiomic nomogram for prediction of major adverse cardiac events in ST-segment elevation myocardial infarction. *Eur Radiol.* 2021;31(2):1140–50. <https://doi.org/10.1007/s00330-020-07176-y>.
 66. Wang J, Bravo L, Zhang J, Liu W, Wan K, Sun J, et al. Radiomics analysis derived from LGE-MRI predict sudden cardiac death in participants with hypertrophic cardiomyopathy. *Front Cardiovasc Med.* 2021;8: 766287. <https://doi.org/10.3389/fcvm.2021.766287>.
 67. Prakken NHJ, Besson FL, Borra RJH, Büther F, Buechel RR, Catana C, et al. PET/MRI in practice: a clinical centre survey endorsed by the European Association of Nuclear Medicine (EANM) and the EANM Forschungs GmbH (EARL). *Eur J Nucl Med Mol Imaging.* 2023;50(10):2927–34. <https://doi.org/10.1007/s00259-023-06308-y>.
 68. Rajiah PS, Kalisz K, Broncano J, Goerne H, Collins JD, François CJ, et al. Myocardial strain evaluation with cardiovascular MRI: physics, principles, and clinical applications. *Radiographics.* 2022;42(4):968–90. <https://doi.org/10.1148/rg.210174>.
 69. Amzulescu MS, De Craene M, Langet H, Pasquet A, Vancraeynest D, Pouleur AC, et al. Myocardial strain imaging: review of general principles, validation, and sources of discrepancies. *Eur Heart J Cardiovasc Imaging.* 2019;20(6):605–19. <https://doi.org/10.1093/ehjci/jez041>.
 70. Wang Y, Sun C, Ghadimi S, Auger DC, Croisille P, Viallon M, et al. StrainNet: improved myocardial strain analysis of cine MRI by deep learning from DENSE. *Radiol Cardiothorac Imaging.* 2023;5(3): e220196. <https://doi.org/10.1148/ryct.220196>.
 71. Wang TKM, Kwon DH, Griffin BP, Flamm SD, Popović ZB. Defining the reference range for left ventricular strain in healthy patients by cardiac MRI measurement techniques: systematic review and meta-analysis. *AJR Am J Roentgenol.* 2020. <https://doi.org/10.2214/ajr.20.24264>.
 72. Oka S, Kai T, Hoshino K, Watanabe K, Nakamura J, Abe M, et al. Effects of empagliflozin in different phases of diabetes mellitus-related cardiomyopathy: a prospective observational study. *BMC Cardiovasc Disord.* 2021;21(1):217. <https://doi.org/10.1186/s12872-021-02024-3>.
 73. Erley J, Genovese D, Tapaskar N, Alvi N, Rashedi N, Besser SA, et al. Echocardiography and cardiovascular magnetic resonance based evaluation of myocardial strain and relationship with late gadolinium enhancement. *J Cardiovasc Magn Reson.* 2019;21(1):46. <https://doi.org/10.1186/s12968-019-0559-y>.
 74. Chen Y, Qian W, Liu W, Zhu Y, Zhou X, Xu Y, et al. Feasibility of single-shot compressed sensing cine imaging for analysis of left ventricular function and strain in cardiac MRI. *Clin Radiol.* 2021. <https://doi.org/10.1016/j.crad.2020.12.024>.
 75. Tian D, Sun Y, Guo JJ, Zhao SH, Lu HF, Chen YY et al. 3.0 T unenhanced Dixon water-fat separation whole-heart coronary magnetic resonance angiography: compressed-sensing sensitivity encoding imaging versus conventional 2D sensitivity encoding imaging. *Int J Cardiovasc Imaging.* 2023. <https://doi.org/10.1007/s10554-023-02878-y>.
 76. Varga-Szemes A, Halfmann M, Schoepf UJ, Jin N, Kilburg A, Dargis DM, et al. Highly accelerated compressed-sensing 4D flow for intracardiac flow assessment. *J Magn Reson Imaging.* 2023;58(2):496–507. <https://doi.org/10.1002/jmri.28484>.
 77. Jenista ER, Wendell DC, Azevedo CF, Klem I, Judd RM, Kim RJ, et al. Revisiting how we perform late gadolinium enhancement CMR: insights gleaned over 25 years of clinical practice. *J Cardiovasc Magn Reson.* 2023;25(1):18. <https://doi.org/10.1186/s12968-023-00925-0>.
 78. Si D, Wu Y, Xiao J, Qin X, Guo R, Liu B, et al. Three-dimensional high-resolution dark-blood late gadolinium enhancement imaging for improved atrial scar evaluation. *Radiology.* 2023;307(5): e222032. <https://doi.org/10.1148/radiol.222032>.
 79. Ohta Y, Tateishi E, Morita Y, Nishii T, Kotoku A, Horinouchi H, et al. Optimization of null point in Look-Locker images for myocardial late gadolinium enhancement imaging using deep learning and a smartphone. *Eur Radiol.* 2023;33(7):4688–97. <https://doi.org/10.1007/s00330-023-09465-8>.
 80. Kato S, Azuma M, Nakayama N, Fukui K, Ito M, Saito N, et al. Diagnostic accuracy of whole heart coronary magnetic resonance angiography: a systematic review and meta-analysis. *J Cardiovasc Magn Reson.* 2023;25(1):36. <https://doi.org/10.1186/s12968-023-00949-6>.
 81. Yue X, Yang L, Wang R, Chan Q, Yang Y, Wu X, et al. The diagnostic value of multiparameter cardiovascular magnetic resonance for early detection of light-chain amyloidosis from hypertrophic cardiomyopathy patients. *Front Cardiovasc Med.* 2022;9:1017097. <https://doi.org/10.3389/fcvm.2022.1017097>.
 82. Agibetov A, Kammerlander A, Duca F, Nitsche C, Koschutnik M, Donà C et al. Convolutional neural networks for fully automated diagnosis of cardiac amyloidosis by cardiac magnetic resonance imaging. *J Pers Med.* 2021;11(12). <https://doi.org/10.3390/jpm11121268>.
 83. Blissett S, Chocron Y, Kovacina B, Afilalo J. Diagnostic and prognostic value of cardiac magnetic resonance in acute myocarditis: a systematic review and meta-analysis. *Int J Cardiovasc Imaging.* 2019;35(12):2221–9. <https://doi.org/10.1007/s10554-019-01674-x>.
 84. Baessler B, Luecke C, Lurz J, Klingel K, Das A, von Roeder M, et al. Cardiac MRI and texture analysis of myocardial T1 and T2 maps in myocarditis with acute versus chronic symptoms of heart failure. *Radiology.* 2019;292(3):608–17. <https://doi.org/10.1148/radiol.2019190101>.
 85. Ojha V, Verma M, Pandey NN, Mani A, Malhi AS, Kumar S, et al. Cardiac magnetic resonance imaging in coronavirus disease 2019 (COVID-19): A systematic review of cardiac magnetic resonance imaging findings in 199 patients. *J Thorac Imaging.* 2021;36(2):73–83. <https://doi.org/10.1097/rti.0000000000000574>.
 86. Vago H, Szabo L, Szabo Z, Ulakcsai Z, Szogi E, Budai G, et al. Immunological response and temporal associations in myocarditis after COVID-19 vaccination using cardiac magnetic resonance imaging: an amplified T-cell response at the heart of it? *Front Cardiovasc Med.* 2022;9: 961031. <https://doi.org/10.3389/fcvm.2022.961031>.

87. Cavalcante JL, Shaw KE, Gössl M. Cardiac magnetic resonance imaging midterm follow up of COVID-19 vaccine-associated myocarditis. *JACC Cardiovasc Imaging*. 2022;15(10):1821–4. <https://doi.org/10.1016/j.jcmg.2022.01.008>.
88. Zhang J, Li Y, Xu Q, Xu B, Wang H. Cardiac magnetic resonance imaging for diagnosis of cardiac sarcoidosis: a meta-analysis. *Can Respir J*. 2018;2018:7457369. <https://doi.org/10.1155/2018/7457369>.
89. Cheung E, Ahmad S, Aitken M, Chan R, Iwanochko RM, Balter M, et al. Combined simultaneous FDG-PET/MRI with T1 and T2 mapping as an imaging biomarker for the diagnosis and prognosis of suspected cardiac sarcoidosis. *Eur J Hybrid Imaging*. 2021;5(1):24. <https://doi.org/10.1186/s41824-021-00119-w>.
90. Aitken M, Chan MV, Urzua Fresno C, Farrell A, Islam N, McInnes MDF, et al. Diagnostic accuracy of cardiac MRI versus FDG PET for cardiac sarcoidosis: a systematic review and meta-analysis. *Radiology*. 2022;304(3):566–79. <https://doi.org/10.1148/radiol.213170>.
91. Xiao Z, Zhong J, Zhong L, Dai S, Lu W, Song L, et al. The prognostic value of myocardial salvage index by cardiac magnetic resonance in ST-segment elevation myocardial infarction patients: a systematic review and meta-analysis. *Eur Radiol*. 2023. <https://doi.org/10.1007/s00330-023-09739-1>.
92. Bodi V, Gavara J, Lopez-Lereu MP, Monmeneu JV, de Dios E, Perez-Sole N, et al. Impact of persistent microvascular obstruction late after STEMI on adverse LV remodeling: a CMR study. *JACC Cardiovasc Imaging*. 2023;16(7):919–30. <https://doi.org/10.1016/j.jcmg.2023.01.021>.
93. Smulders MW, Van Assche LMR, Bekkers S, Nijveldt R, Beijinck CWH, Kim HW, et al. Epicardial surface area of infarction: a stable surrogate of microvascular obstruction in acute myocardial infarction. *Circ Cardiovasc Imaging*. 2021;14(2): e010918. <https://doi.org/10.1161/circimaging.120.010918>.
94. Cha MJ, Lee JH, Jung HN, Kim Y, Choe YH, Kim SM. Cardiac magnetic resonance-tissue tracking for the early prediction of adverse left ventricular remodeling after ST-segment elevation myocardial infarction. *Int J Cardiovasc Imaging*. 2019;35(11):2095–102. <https://doi.org/10.1007/s10554-019-01659-w>.
95. Leung SW, Charnigo RJ, Ratajczak T, Abo-Aly M, Shokri E, Abdel-Latif A, et al. End-systolic circumferential strain derived from cardiac magnetic resonance feature-tracking as a predictor of functional recovery in patients with ST-segment elevation myocardial infarction. *J Magn Reson Imaging*. 2021;54(6):2000–3. <https://doi.org/10.1002/jmri.27772>.
96. Cui J, Zhao Y, Qian G, Yue X, Luo C, Li T. Cardiac magnetic resonance for the early prediction of reverse left ventricular remodeling in patients with ST-segment elevation myocardial infarction. *Eur Radiol*. 2023. <https://doi.org/10.1007/s00330-023-09907-3>.
97. Wang J, Meng Y, Han S, Hu C, Lu Y, Wu P, et al. Predictive value of total ischaemic time and T1 mapping after emergency percutaneous coronary intervention in acute ST-segment elevation myocardial infarction. *Clin Radiol*. 2023. <https://doi.org/10.1016/j.crad.2023.06.010>.
98. Bergamaschi L, Foà A, Paolisso P, Renzulli M, Angeli F, Fabrizio M, et al. Prognostic role of early cardiac magnetic resonance in myocardial infarction with nonobstructive coronary arteries. *JACC Cardiovasc Imaging*. 2023. <https://doi.org/10.1016/j.jcmg.2023.05.016>.
99. Li XM, Jiang L, Min CY, Yan WF, Shen MT, Liu XJ, et al. Myocardial perfusion imaging by cardiovascular magnetic resonance: research progress and current implementation. *Curr Probl Cardiol*. 2023;48(6): 101665. <https://doi.org/10.1016/j.cpcardiol.2023.101665>.
100. Rahman H, Scannell CM, Demir OM, Ryan M, McConkey H, Ellis H, et al. High-resolution cardiac magnetic resonance imaging techniques for the identification of coronary microvascular dysfunction. *JACC Cardiovasc Imaging*. 2021;14(5):978–86. <https://doi.org/10.1016/j.jcmg.2020.10.015>.
101. Jogiya R, Kozerke S, Morton G, De Silva K, Redwood S, Perera D, et al. Validation of dynamic 3-dimensional whole heart magnetic resonance myocardial perfusion imaging against fractional flow reserve for the detection of significant coronary artery disease. *J Am Coll Cardiol*. 2012;60(8):756–65. <https://doi.org/10.1016/j.jacc.2012.02.075>.
102. Károlyi M, Gotschy A, Polacin M, Plein S, Paetsch I, Jahnke C, et al. Diagnostic performance of 3D cardiac magnetic resonance perfusion in elderly patients for the detection of coronary artery disease as compared to fractional flow reserve. *Eur Radiol*. 2023;33(1):339–47. <https://doi.org/10.1007/s00330-022-09040-7>.
103. Arai AE, Schulz-Menger J, Shah DJ, Han Y, Bandettini WP, Abraham A, et al. Stress perfusion cardiac magnetic resonance vs SPECT imaging for detection of coronary artery disease. *J Am Coll Cardiol*. 2023;82(19):1828–38. <https://doi.org/10.1016/j.jacc.2023.08.046>.
104. Wang S, Patel H, Miller T, Ameyaw K, Miller P, Narang A, et al. Relation of myocardial perfusion reserve and left ventricular ejection fraction in ischemic and nonischemic cardiomyopathy. *Am J Cardiol*. 2022;174:143–50. <https://doi.org/10.1016/j.amjcard.2022.02.022>.
105. Nagel E, Carerj ML, Arendt CT, Puntmann VO. After ISCHEMIA: is cardiac MRI a reliable gatekeeper for invasive angiography and myocardial revascularization? *Herz*. 2020;45(5):446–52. <https://doi.org/10.1007/s00059-020-04936-w>.
106. Nagel E, Greenwood JP, McCann GP, Bettencourt N, Shah AM, Hussain ST, et al. Magnetic resonance perfusion or fractional flow reserve in coronary disease. *N Engl J Med*. 2019;380(25):2418–28. <https://doi.org/10.1056/NEJMoa1716734>.
107. Miller CD, Mahler SA, Snively AC, Raman SV, Caterino JM, Clark CL, et al. Cardiac magnetic resonance imaging versus invasive-based strategies in patients with chest pain and detectable to mildly elevated serum troponin: a randomized clinical trial. *Circ Cardiovasc Imaging*. 2023;16(6): e015063. <https://doi.org/10.1161/circimaging.122.015063>.
108. Ommen SR, Mital S, Burke MA, Day SM, Deswal A, Elliott P, et al. 2020 AHA/ACC Guideline for the diagnosis and treatment of patients with hypertrophic cardiomyopathy: a report of the American College of Cardiology/American Heart Association Joint Committee on Clinical Practice Guidelines. *Circulation*. 2020;142(25):e558–631. <https://doi.org/10.1161/cir.0000000000000937>.
109. Freitas P, Ferreira AM, Arteaga-Fernández E, de Oliveira AM, Mesquita J, Abecasis J, et al. The amount of late gadolinium enhancement outperforms current guideline-recommended criteria in the identification of patients with hypertrophic cardiomyopathy at risk of sudden cardiac death. *J Cardiovasc Magn Reson*. 2019;21(1):50. <https://doi.org/10.1186/s12968-019-0561-4>.
110. Suwa K, Sato R, Iguchi K, Maekawa Y. Four-dimensional flow cardiac MRI for hemodynamic assessment of alcohol septal ablation for hypertrophic obstructive cardiomyopathy with multiple obstructions. *Radiology: Cardiothoracic Imaging*. 2023;5(5):230074. <https://doi.org/10.1148/ryct.230074>.
111. Becker MAJ, van der Lingen ACJ, Cornel JH, van de Ven PM, van Rossum AC, Allaart CP, et al. Septal midwall late gadolinium enhancement in ischemic cardiomyopathy and nonischemic dilated cardiomyopathy-characteristics and prognosis. *Am J Cardiol*. 2023;201:294–301. <https://doi.org/10.1016/j.amjcard.2023.06.042>.

112. Yuan Y, Sun J, Jin D, Zhao S. Quantitative left ventricular mechanical dyssynchrony by magnetic resonance imaging predicts the prognosis of dilated cardiomyopathy. *Eur J Radiol.* 2023;164: 110847. <https://doi.org/10.1016/j.ejrad.2023.110847>.
113. Liu T, Zhou Z, Bo K, Gao Y, Wang H, Wang R, et al. Association between left ventricular global function index and outcomes in patients with dilated cardiomyopathy. *Front Cardiovasc Med.* 2021;8: 751907. <https://doi.org/10.3389/fcvm.2021.751907>.
114. Shen MT, Li Y, Guo YK, Gao Y, Jiang L, Shi R, et al. The impact of hypertension on left ventricular function and remodeling in non-ischemic dilated cardiomyopathy patients: A 3.0 T MRI Study. *J Magn Reson Imaging.* 2023;58(1):159–71. <https://doi.org/10.1002/jmri.28475>.
115. Seraphim A, Westwood M, Bhuva AN, Crake T, Moon JC, Meneses LJ, et al. Advanced imaging modalities to monitor for cardiotoxicity. *Curr Treat Options Oncol.* 2019;20(9):73. <https://doi.org/10.1007/s11864-019-0672-z>.
116. Galán-Arriola C, Lobo M, Vélchez-Tschischke JP, López GJ, de Molina-Iracheta A, Pérez-Martínez C, et al. Serial magnetic resonance imaging to identify early stages of anthracycline-induced cardiotoxicity. *J Am Coll Cardiol.* 2019;73(7):779–91. <https://doi.org/10.1016/j.jacc.2018.11.046>.
117. Mahmood SS, Fradley MG, Cohen JV, Nohria A, Reynolds KL, Heinzerling LM, et al. Myocarditis in patients treated with immune checkpoint inhibitors. *J Am Coll Cardiol.* 2018;71(16):1755–64. <https://doi.org/10.1016/j.jacc.2018.02.037>.
118. Mabudian L, Jordan JH, Bottinor W, Hundley WG. Cardiac MRI assessment of anthracycline-induced cardiotoxicity. *Front Cardiovasc Med.* 2022;9: 903719. <https://doi.org/10.3389/fcvm.2022.903719>.
119. Jang SY, Kim J, Kim YS, Chang YA, Jung W, Kim HO et al. Clinical features and test indications of 11,087 patients undergoing cardiac magnetic resonance imaging during a decade in a tertiary referral center: a retrospective observational study. *Precis Future Med.* 2023;7(2):62–73. <https://doi.org/10.23838/pfm.2023.00023>.
120. Kozor R, Walker S, Parkinson B, Younger J, Hamilton-Craig C, Selvanayagam JB, et al. Cost-effectiveness of cardiovascular magnetic resonance in diagnosing coronary artery disease in the Australian health care system. *Heart Lung Circ.* 2021;30(3):380–7. <https://doi.org/10.1016/j.hlc.2020.07.008>.
121. Kwong RY, Ge Y, Steel K, Bingham S, Abdullah S, Fujikura K, et al. Cardiac magnetic resonance stress perfusion imaging for evaluation of patients with chest pain. *J Am Coll Cardiol.* 2019;74(14):1741–55. <https://doi.org/10.1016/j.jacc.2019.07.074>.
122. Pontone G, Andreini D, Guaricci AI, Rota C, Guglielmo M, Mushtaq S et al. The STRATEGY Study (Stress Cardiac Magnetic Resonance Versus Computed Tomography Coronary Angiography for the Management of Symptomatic Revascularized Patients): resources and outcomes impact. *Circ Cardiovasc Imaging.* 2016;9(10). <https://doi.org/10.1161/CIRCIMAGING.116.005171>.
123. Hegde VA, Biederman RW, Mikolich JR. Cardiovascular magnetic resonance imaging-incremental value in a series of 361 patients demonstrating cost savings and clinical benefits: an outcome-based study. *Clin Med Insights Cardiol.* 2017;11:1179546817710026. <https://doi.org/10.1177/1179546817710026>.

Publisher's Note Springer Nature remains neutral with regard to jurisdictional claims in published maps and institutional affiliations.

Springer Nature or its licensor (e.g. a society or other partner) holds exclusive rights to this article under a publishing agreement with the author(s) or other rightsholder(s); author self-archiving of the accepted manuscript version of this article is solely governed by the terms of such publishing agreement and applicable law.